Structural evolution of Andros (Cyclades, Greece): a key to the behaviour of a (flat) detachment within an extending continental crust

C. Mehl, L. Jolivet, O. Lacombe, L. Labrousse and G. Rimmele

Geological Society, London, Special Publications 2007; v. 291; p. 41-73
doi:10.1144/SP291.3

Structural evolution of Andros (Cyclades, Greece): a key to the behaviour of a (flat) detachment within an extending continental crust

C. MEHL[1], L. JOLIVET[1], O. LACOMBE[1], L. LABROUSSE[1] & G. RIMMELE[2]

[1]*Laboratoire de Tectonique, UMR 7072, Université Pierre et Marie Curie, T 46-00 E2, case 129, 4 place Jussieu, 75252 Paris Cedex 05, France (e-mail: caroline.mehl@lgs.jussieu.fr)*

[2]*Laboratoire de Géologie, UMR 8538, Ecole Normale Supérieure, 24, rue Lhomond, 75005 Paris, France*

Abstract: The continental crust extends in a brittle manner in its upper part and in more distributed (ductile) manner in its lower part. During exhumation of HP metamorphic rocks, brittle features superimpose on earlier ductile ones as a result of the progressive localization of deformation. The islands of Tinos and Andros are part of the numerous metamorphic core complexes exhumed in the Aegean domain. They illustrate two steps of a gradient of finite extension along a transect between Mt. Olympos and Naxos. This study confirms the main role of boudinage as an initial localizing factor at the brittle–ductile transition and emphasizes the continuum of strain from ductile to brittle during exhumation. Early low-angle semi-brittle shear planes superimpose onto precursory ductile shear bands, whereas steeply dipping late brittle planes develop by progressive steepening of structures or sliding across en echelon arrays of veins. The comparison between Tinos and Andros allows us to propose a complete dynamic section of the Aegean extending continental crust and emphasizes that the strain localization process depends on both its rheological stratification and its compositional heterogeneity.

Although post-orogenic extension has been studied for a long time in several regions of the world, such as the Basin and Range Province and the Aegean Sea, numerous questions remain open.

It is commonly admitted that the extending continental crust is characterized by steeply dipping normal faults in its upper part (Jackson 1987; Jackson & White 1989), crustal-scale shear bands at and below the brittle–ductile transition and more distributed ductile deformation in its lower part. Such a model raises two main problems: (1) the initial localizing factor allowing localization of deformation at the brittle–ductile transition zone although, considering the rheological envelopes, a maximum of strength is expected there; (2) the way in which ductile structures evolve towards brittle ones when the rocks pass through the brittle–ductile transition zone.

Metamorphic core complexes (MCC), because they offer the opportunity to observe large portions of the exhumed lower continental crust, are good sites to study the way in which deformation localizes and evolves from ductile to brittle. MCCs were recognized on several islands in the Aegean region during the last 20 years (Lister *et al.* 1984; Avigad & Garfunkel 1989, 1991; Gautier & Brun 1994*a*; Avigad *et al.* 1997). (Jolivet & Patriat (1999) studied a transect starting in the Mt. Olympos region and running through the MCCs of Evia, Andros, Tinos, Mykonos, Paros and Naxos. They concluded that the Aegean metamorphic core complexes are characterized by a gradient of finite extension from continental Greece towards the centre of the Cyclades, maximum extension being observed on the island of Naxos.

Several detailed structural studies were carried out on Tinos. They allowed researchers to emphasize the role of boudinage as an initial efficient localizing factor (Jolivet *et al.* 2004*a*) and to propose a new scenario of evolution of deformation from ductile to brittle (Mehl *et al.* 2005). Despite its key position on the Mt. Olympos–Naxos transect and its situation in the direct vicinity of Tinos, little attention has been paid to the structural framework of Andros. The aim of this study is twofold. First, we present the results of structural fieldwork carried out on Andros, with special emphasis on the progressive evolution of structures from ductile to brittle when rocks in the footwall of the main detachment are exhumed. Field observations allow us to test the mechanism of initiation of ductile deformation first proposed on Tinos and to emphasize the role played by boudinage. Second, we compare the extensional structures of Andros and Tinos, which are situated close to each other. The gradient of extension gives access to different portions of the extending continental crust, from the deeper and more stretched parts in the central

From: TAYMAZ, T., YILMAZ, Y. & DILEK, Y. (eds) *The Geodynamics of the Aegean and Anatolia.* Geological Society, London, Special Publications, **291**, 41–73.
DOI: 10.1144/SP291.3 0305-8719/07/$15.00

Aegean (Naxos and Paros), to the shallower parts near the continent (Tinos and Andros). Studying and comparing Andros with Tinos could lead to the development of a more complete scheme of evolution of a previously thickened continental crust, extending at the brittle–ductile transition.

The localization process: previous studies

Several studies have already been carried out on the localizing factors and the localization process, especially on Tinos. They are summarized below.

Localizing factors

Because localization of deformation occurs at the brittle–ductile transition, where the rheological envelopes predict a maximum of strength, the localization process requires localization factors that induce a local decrease of strength, making the onset of shear bands feasible.

Three localizing factors reducing the deviatoric stress at the brittle–ductile transition are classically described in the literature: increasing temperature (Kirby 1985), dynamic recrystallization and softening reactions, such as, for example, breakdown of strong feldspars to weaker white micas (Mitra 1978; White & Knipe 1978; Dixon & Williams 1983; Marquer *et al.* 1985; Fitz Gerald & Stünitz 1993; Wintsch *et al.* 1995; Wibberly 1999; Gueydan *et al.* 2001, 2003). None of these factors seems to be convenient in the case of the Cyclades: temperature does not play an important role at the brittle–ductile transition, being more efficient at the base of the crust (Kirby 1985). Dynamic recrystallization occurs only after large strains (Weathers *et al.* 1979) and thus cannot be involved in the initiation of shear bands. Finally, replacement of feldspars by micas cannot be advocated here because Cycladic blueschists are initially very rich in phyllosilicates and no significant increase in the concentration of micas can be observed during deformation. An additional localizing factor has been proposed by Jolivet *et al.* (2004*a*): boudinage. Metamorphic core complexes were first interpreted in terms of mega-boudinage in the Basin and Range Province by Davis & Coney (1979) and Davis (1980), but Jolivet *et al.* (2004*a*) pointed out the relation between boudinage and localization of shear bands. Boudinage induces progressive localization of strain in interboudin necks, which finally leads to local stress concentration and higher strain rate. When reaching the brittle–ductile transition, the first localized structures, such as shear bands and faults, will form in the necks between boudins. This mechanism of localization, based on field observations on Tinos, fits observations at metre scale as well as at crustal scale. The efficiency of this localizing factor will be tested from new field observations on Andros.

The localization process: the example of Tinos

Metamorphic core complexes are composed of two tectonic units separated by shallow-dipping detachments. Upper units display brittle steeply dipping extensional structures characteristic of the upper continental crust. Lower units have been exhumed along the detachments and underwent successively ductile and brittle deformation during their way back to the surface (Gautier & Brun 1994*b*; Jolivet & Patriat 1999; Jolivet *et al.* 2004*a*). They are therefore characterized by a superimposition of ductile and brittle structures, as a consequence of progressive localization of deformation during exhumation (Mehl *et al.* 2005). Detachments are considered as the ultimate evolution of shear bands towards more localized deformation (Lister & Davis 1989).

A detailed study of both ductile and brittle features in the footwall of the Tinos detachment allowed Mehl *et al.* (2005) to demonstrate a continuum of strain from ductile to brittle during extensional kinematics and exhumation of HP metamorphic rocks. Brittle extensional structures are characterized, on Tinos, by shallow- and steeply dipping normal faults; both types have formed under a vertical shortening axis, as shown by their association with ubiquitous vertical veins and as confirmed by inversions of fault slip data. The only way to explain the initiation of low-angle brittle extensional structures (including the detachment) is that the main displacement along the detachment was accommodated by ductile deformation and cataclastic flow, only the last increment of deformation being accommodated in a purely brittle manner (Mehl *et al.* 2005).

Tinos and Andros, because they are situated close to each other, have the same kinematic history. Moreover, they are situated on a gradient of finite strain. The comparison of the structures of the two islands could lead us to build a more complete section of the extending continental crust.

Structural setting of Andros

The Aegean domain

Andros is situated in the northern part of the Aegean Sea, which formed in the back-arc of the Hellenic subduction zone (Le Pichon & Angelier 1981) in a region once occupied by the Hellenides–Taurides mountain belt (Aubouin & Dercourt 1965; Brunn

et al. 1976; Jacobshagen *et al.* 1978). Post-orogenic extension dates back to the late Oligocene–earliest Miocene, as shown by the cooling ages of the metamorphic core complexes and the ages of the basins in the region (Lister *et al.* 1984; Gautier & Brun 1994*a*; Jolivet *et al.* 1994; Jolivet & Faccenna 2000), and affected the whole Aegean domain. It is now localized around the Aegean Sea, in west Turkey, in the Peloponnesus, in the Gulf of Corinth and in Crete (Seyitoglu & Scott 1991, 1996; Taymaz *et al.* 1991; Armijo *et al.* 1992, 1996; Rietbrock *et al.* 1996; Rigo *et al.* 1996; Taymaz *et al.* 2004).

As mentioned above, several MCCs were recognized in the Aegean region during the last 20 years (Lister *et al.* 1984; Avigad & Garfunkel 1989, 1991; Gautier & Brun 1994*a*; Avigad *et al.* 1997). Two types of domes have been described by Jolivet *et al.* (2004*a*) in the basin: 'b-type' domes (Tinos and Andros), having their axis perpendicular to extension, and 'a-type' (Paros, Naxos and Mykonos) domes, elongated parallel to extension. The 'b-type' domes were exhumed *c.* 5 Ma before the 'a-type' domes. The 'a-type' domes correspond to exhumation of deeper and higher-temperature levels of crust and have recorded a constrictional component of deformation shown by north–south-trending fold axes. The main direction of extension is north–south to NE–SW over the entire area.

The Aegean domain is cut by several major NE-dipping normal faults (Taymaz *et al.* 1991, 1994; Jackson 1994) isolating crustal-scale tilted blocks (Papanikolaou *et al.* 1988; Jolivet *et al.* 1994), whose geometry is consistent with crustal-scale boudinage (Fig. 1). Andros belongs to the same block as Evia, Tinos and Mykonos.

Previous studies

A complete morphological study of Andros has already been made by Papanikolaou (1978). The topography of the island shows a structural dome oriented NW–SE (Fig. 1) in continuity with Evia and Tinos. It consists of a succession of NE–SW-trending mountains and valleys. The topography is asymmetric, with sharp slopes on the southern coast of the island and smoother ones on the northern coast, as shown by the topographic profile (Fig. 1, section AA′). The topography is smoother in the northwestern part of the island.

The structural framework of the island has been interpreted as reflecting mega-folds with NE–SW axes (Papanikolaou 1978). The smoother relief in the NW seems to correspond to what has been identified by Papanikolaou (1978) as a separate structural unit, the Makrotantalon Unit; this will be discussed in a later section. This attenuation must be due to differential erosion testifying to a 'weaker' lithology in the western part of the island. In contrast, the sharpness of the southern coast can probably be explained by the presence of an offshore normal fault, dipping to the SW (Fig. 1; map of the Aegean Sea).

Two tectonic units, separated by ophiolites that underline a presumable NE-dipping thrust, were originally described on Andros (see Fig. 2; Papanikolaou 1978; Reinecke *et al.* 1985). The Upper Unit, or Makrotantalon Unit, crops out in the northwestern part of the island. The occurrence of fauna relics in the Makrotantalon Unit supports a Permian age of sedimentation (Papanikolaou 1978). The Lower Unit, or Central Unit, is expected to be of Mesozoic age (Reinecke 1982). Both units are composed of an alternation of metabasites, metapelites and marble horizons, as on Tinos. Manganese-rich minerals have been described in the Central Unit (Reinecke 1982). Serpentinite bodies have been mapped on the northern coast of the island within this unit. Their significance will be discussed below.

The main part of the island has been retromorphosed to greenschist facies. (Reinecke 1982) deduced, from the reaction celsian + water = cymrite, a temperature of 400 °C and a pressure of 5–6 kbar for the greenschist event. Concerning the Makrotantalon Unit, Papanikolaou (1978) described garnet in the lowest horizon of the metapelites and Reinecke (1982) pointed out relics of omphacite and chloromelanite in the metabasites. Garnet and glaucophane are preserved in the metabasites of the Central Unit (Papanikolaou 1978). HP relics are better preserved on the southern coast of the island. Peak P–T conditions are estimated at 450–500 °C and >10 kbar from the reaction of sursassite-bearing to spessartine-bearing assemblages of the manganese-rich layers of the Central Unit (Reinecke 1986).

Andros as a metamorphic core complex

Lister *et al.* (1984) first described metamorphic core complexes in the Aegean Sea on the islands of Naxos and Ios. They suggested that the shallow-dipping faults separating the HP–LT rocks of the Cycladic Blueschist Belt (CBB) from non-metamorphosed ophiolites of Pelagonian affinity could be normal faults, and not thrust faults as previously proposed. They proposed that the exhumation of HP–LT metamorphic rocks could be explained by the presence of a south-dipping low-angle normal fault (or detachment) above the CBB. Faure & Bonneau (1988) further pointed out a top-to-the-NE sense of shear on Mykonos suggesting that the detachment there was not south-dipping, but rather NE-dipping. Following this dynamics, Avigad & Garfunkel (1989) described a NE-dipping detachment on Tinos that separates a

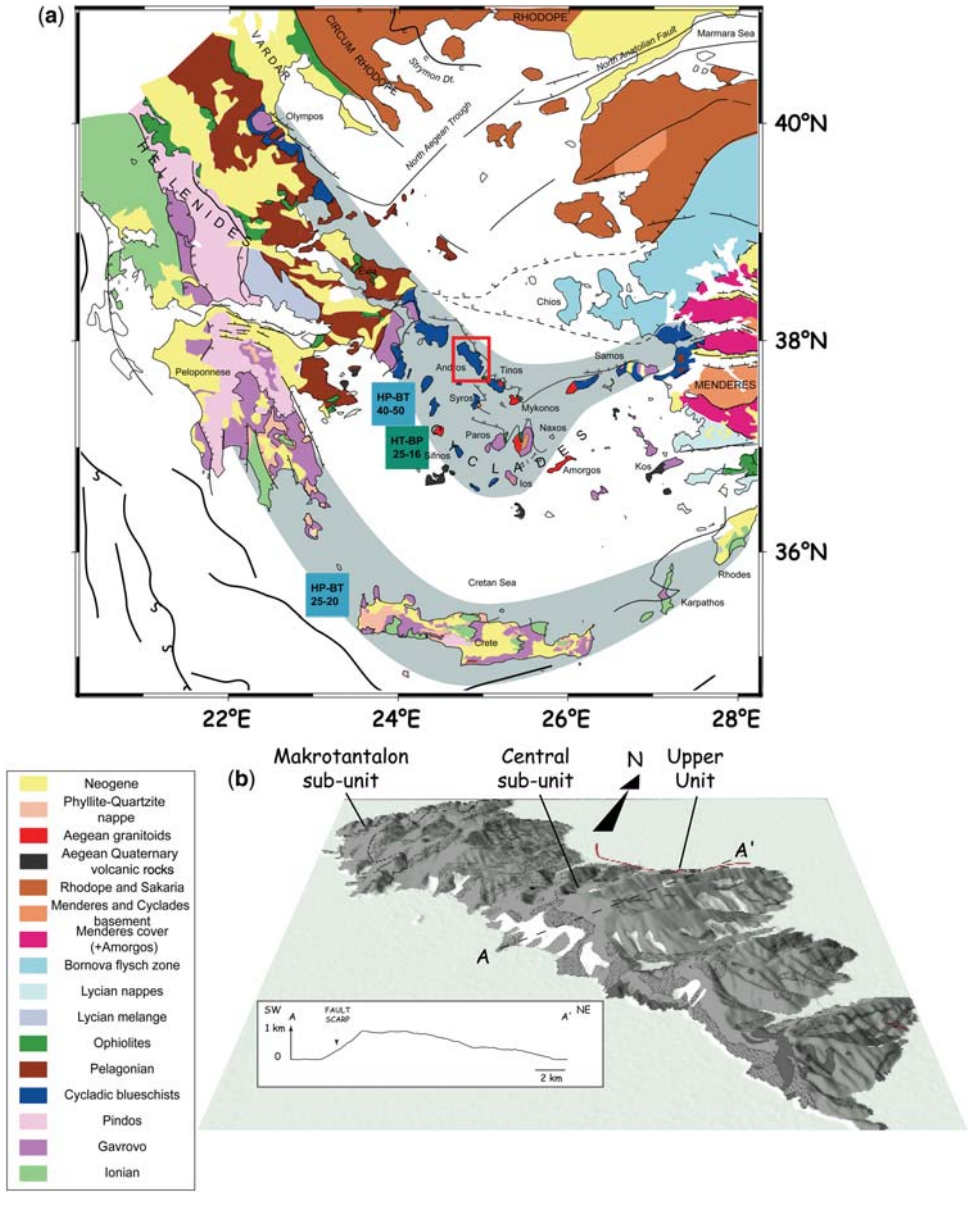

Fig. 1. (**a**) Geological map of the Aegean domain, after Jolivet *et al.* (2004a) The two blueschist belts of the domain are shown in blue–grey. The northern one corresponds to the Cycladic Blueschist Belt (CBB). (**b**) SRTM topographic model of Andros, ×2 vertical exaggeration. The island has been identified as being part of the CBB. The geological map of the island has been overlain on the topography (geological background: same key as in Fig. 2). AA': SW–NE topographic section of the island. The southern coast of the island is affected by a fault scarp. The overall morphology of the island has been related to megafolds with NE–SW axes.

Lower Unit of metamorphic rocks from an upper unit that is affected neither by the Eocene HP event nor by the Oligo-Miocene greenschist overprint. The kinematics of this extensional episode on Tinos was first described by Gautier & Brun (1994*a*, *b*) and Patriat & Jolivet (1998).

Such a vertical succession has been identified on Andros by Patriat (1996). What had been previously

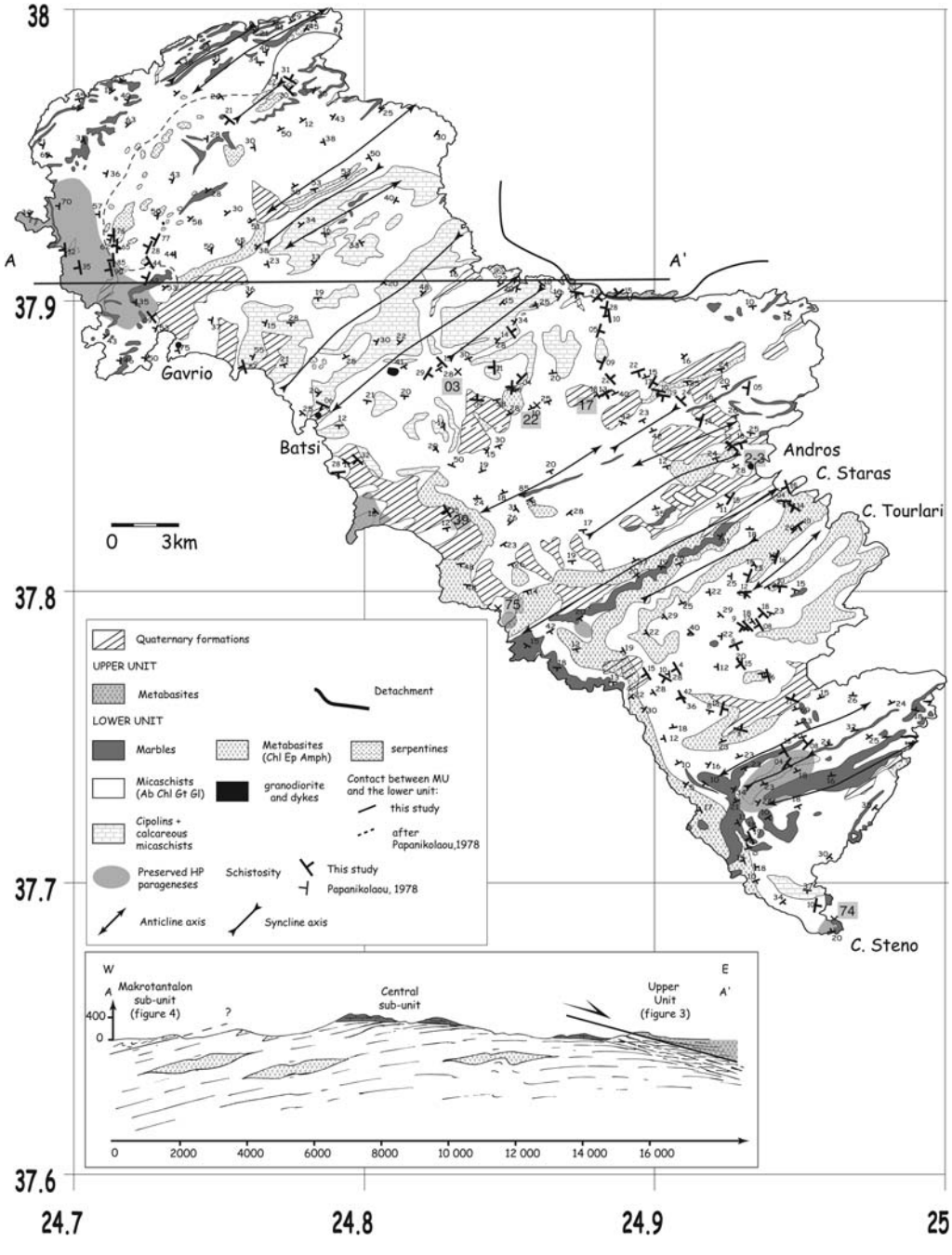

Fig. 2. Geological map of Andros. Two tectonic units are identified, separated by a low-angle detachment. Preserved blueschist parageneses, direction and plunge of schistosity, and ductile megafold NE–SW axes are shown. AA′: conceptual cross-section of the island. Two gradients exist on Andros from SW to NE: a gradient of retrogression and a gradient of finite strain. The closer the detachment, the more retrogressed the rocks and the less coaxial (that is, the more intense) the deformation. Deformation is accommodated, on the northeasternmost part of the island, by localized decametre-scale shear bands.

mapped by Papanikolaou (1978) as a serpentinite body within the Lower Unit and cropping out on the northern coast of the island could be recognized as the upper unit of a metamorphic core complex (Fig. 3). The Upper Unit of Andros is separated by a low-angle normal fault from the Lower Unit (Fig. 3). The contact is underlined by a discontinuous reddish breccia, as on Tinos.

The detachment

The detachment is visible along the NE coast of Andros below two remnants of the Upper Unit on two capes on either side of the wrecked ship *Semiramis*. The Upper Unit is composed of intensely foliated greenschists and serpentinites. A shallow NE-dipping normal fault marks the contact (Fig. 3) and shallow-dipping minor normal faults root in the underlying breccia (Fig. 3d). The basal breccia is stratified, with a 3–5 m thick reddish breccia made of serpentinite clasts resting on top of a 10 m thick greenish serpentinite breccia overlying highly sheared serpentinites mixed with some pelitic schists from the Lower Unit (Fig. 3c). The whole system of breccia rests on top of the sheared schists of the Lower Unit. The direction of slip along the faults in the contact is toward the NE, and semi-ductile features such as sigmoidal schistosity in the cataclasites also indicate top-to-the-NE shear.

In summary, Andros is composed of two structural units separated by a flat-lying detachment, in the sense of metamorphic core complexes. The unmetamorphosed Upper Unit crops out only in a small area on the northern coast of the island. The Lower Unit, metamorphosed under Eocene HP–LT conditions and retromorphosed to greenschist facies during post-orogenic extension, crops out on the major part of the island. Bröcker & Franz (2007) recently performed a Rb–Sr phengite dating on the Lower Unit. The study yielded, as it is common in the Cyclades, an HP–LT event at *c*. 50 Ma and a second retrogression episode at *c*. 20 Ma.

Relics of blueschist facies recorded on Andros are considered to correspond to the Eocene HP event responsible of the formation of the Cycladic Blueschist Belt. Within this framework, the actual significance of the Makrotantalon Unit as a sub-unit thrust onto the main part of the island deserves consideration.

The Makrotantalon Unit

The origin and structural significance and position of the Makrotantalon Unit have been a matter of debate. Assuming the presence of a tectonic contact at the base of the Makrotantalon Unit, two hypotheses can be made on its origin. Some workers (Papanikolaou 1978, 1987; Shaked *et al.* 2000) consider it as part of the Ochi Unit that crops out on the nearby island of Evia. This interpretation implicitly supposes that it is part of the Cycladic Blueschist unit and that it has recorded an HP–LT event of Eocene age. Other workers (Blake *et al.* 1981; Bonneau 1982; Dürr 1986) consider it as part of the Pelagonian domain or as the Upper Unit of the metamorphic core complex (Katzir *et al.* 2000). Assuming a structural definition of the Pelagonian domain, and thus referring it to the late Jurassic ophiolite obduction and associated deformation (Bonneau 1982; Jolivet *et al.* 2004*b*), implicitly supposes that the rocks of the Makrotantalon Unit did not record any Tertiary high-pressure metamorphism.

The Rb–Sr phengite dating by Bröcker & Franz (2007) shows that the Makrotantalon Unit has preserved ages as old as 100 Ma as well as a more recent episode at 20 Ma. This suggests that the Makrotantalon Unit has not recorded the high-pressure event recorded in the Lower Unit at 50 Ma. However, in the field, the contact between the Makrotantalon Unit and the Lower Unit is not clear, except in one outcrop on the northern part of the island. The contact was mapped in a different position by Papanikolaou (1978) and Bröcker & Franz (2007) and we were unable to identify a clear detachment surface similar to those observed on Tinos or on the NE coast of Andros. Some researchers have cast doubt on the existence of the contact (Gautier 1994; Patriat 1996). Two alternative solutions are thus available: (1) the Makrotantalon Unit is part of the Cycladic Blueschists and has escaped re-equilibration in the blueschist facies for some unknown reason; (2) the Makrotantalon Unit is an intermediate unit juxtaposed between the Upper Cycladic Unit and the Lower Unit.

Structures in the footwall of the detachment

Rocks of the Lower Unit underwent first an Eocene HP–LT metamorphic event characteristic of the Hellenides and then an Oligo-Miocene retrogression to greenschist facies during exhumation. During their exhumation, rocks passed through the brittle–ductile transition: brittle features were thus superimposed on ductile ones. We describe below the ductile and brittle extensional structures.

From blueschist- to greenschist-facies deformation

HP relics and syn-HP ductile structures are better preserved on the southern coast of the island west

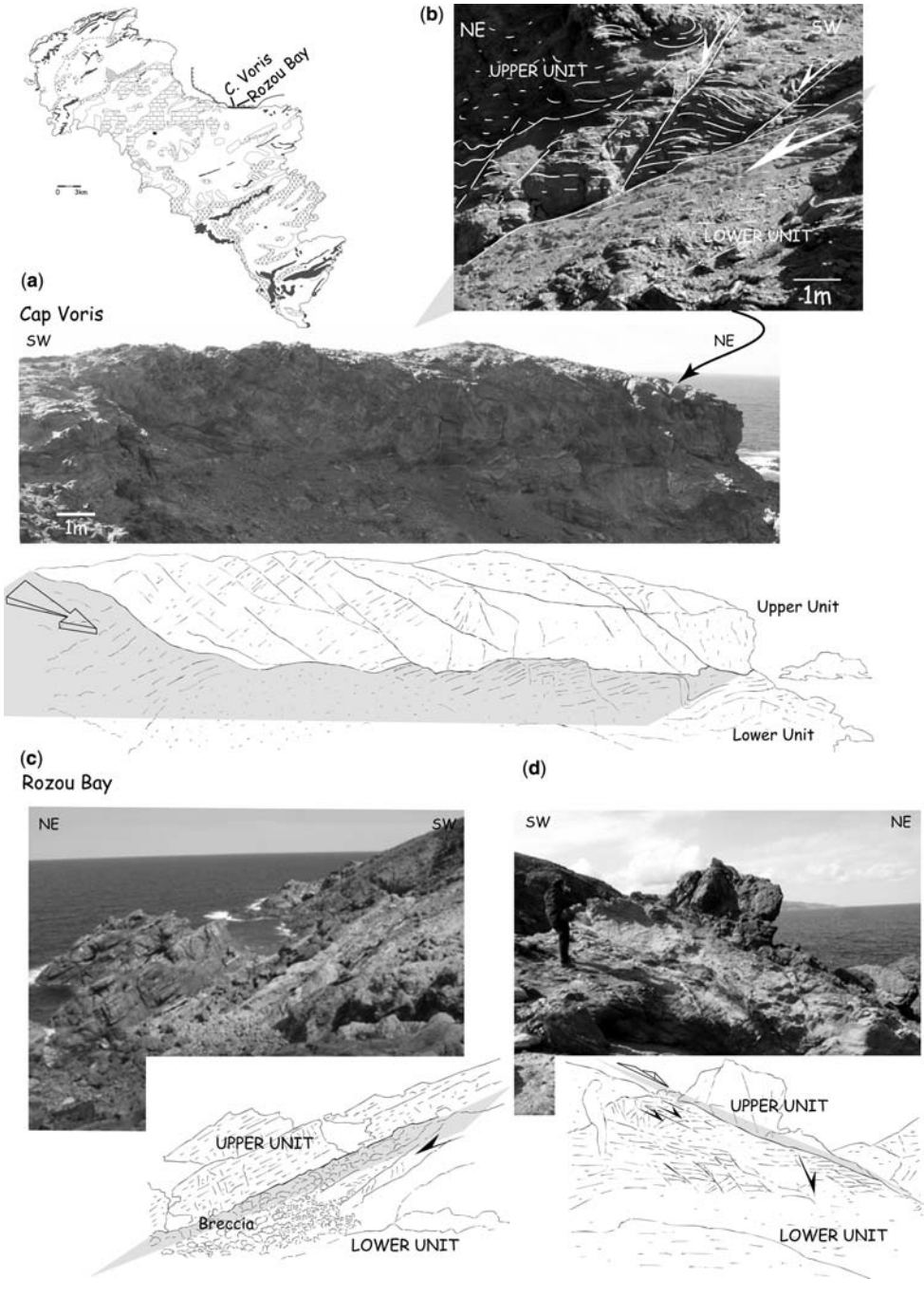

Fig. 3. Hanging wall and the Andros detachment. The hanging wall is composed essentially of greenschists and serpentinites. (**a**) Shallow-dipping normal fault that separates the Upper Unit from the Lower Unit at Cap Voris. The Upper Unit is affected by steeply dipping normal faults. (**b**) Close-up view of the steeply dipping normal faults affecting the Upper Unit at Cap Voris. (**c**) The detachment in Rozou Bay. The contact is sealed by a reddish breccia of serpentinite clasts resting on a greenish breccia of serpentinites. Normal faults have developed in the breccia. The normal sense of motion along the detachment is shown by the sigmoidal schistosity in the cataclasites, which indicates top-to-the-NE shear. (**d**) Both the Upper Unit and the breccia are affected by a dense network of steeply dipping normal faults and veins.

of Gavrio. They are also present sporadically in the Lower Unit especially along the southern coast of the island (Ipsili and Thiaki capes) and locally within metabasite boudins dispersed over the island. HP relics mainly consist of garnet relics or glaucophane-bearing mineral assemblages. Locations of preserved HP parageneses are shown on the geological map of the island (Fig. 2).

A section west of Gavrio shows the progressive evolution of deformation from the blueschist stage to the greenschist retrogression (Fig. 4). Table 1 summarizes this evolution.

The section shows rather well-preserved blueschist-facies metapelites with garnet and glaucophane and glaucophane-rich lenses of metabasites embedded within an alternation of retrograded metapelites and marbles. The best-preserved blueschists are found in the southeastern part of the section on either side of a highly deformed serpentinite lens. Whether this serpentinite represents the trace of a former thrust contact is difficult to ascertain because the lithologies below and above the contact are not very different. The preservation of the high-pressure S_1 foliation below and above the serpentinite lens may be related to the low resistance of the serpentinite that has taken up all the retrograde deformation and thus 'prevented' surrounding rocks deforming, but this hypothesis remains to be ascertained.

This section shows an intense retrograde greenschist-facies deformation that is also ubiquitous in the rest of the island (see below). The HP S_1 foliation is first reworked by P_2 folds and S_2 crenulation cleavage. With increasing shear strain, S_2 and L_2 become more intense and P_2 folds evolve toward sheath folds. This evolution is coeval with greenschist retrogression.

Near the top of the section intensely foliated and folded blue marbles (Fig. 4e) crop out before a west-dipping normal fault. The section ends near Agios Sostis, where dolomitic marbles rest on top of the section above albitic schists. The NW part of the section is cut by several normal faults of various sizes.

Greenschist finite deformation

The S_2 schistosity and the L_2 stretching lineation have been mapped all over the island (Figs 2 and 5). Orientations and dips of schistosity show a succession of kilometre-scale NE–SW folds, already described by Papanikolaou (1978). The stretching lineation shows a remarkable consistency throughout the island with a NE–SW trend with only local distortions, especially west of Gavrio, where it trends more north–south. Because both the stretching lineation and the fold axes show a consistent NE–SW trend (map in Fig. 5), it is difficult to ascertain the chronology of folding, stretching and shearing. Tilting of both schistosity and late normal fault systems nevertheless suggests that folding may have occurred during the latest greenschist evolution. Such folding could correspond to a component of constriction during extension. Such a component of constriction has already been recorded on Tinos (Mehl *et al.* 2005) and in the Menderes Massif, in western Turkey (Bozkurt & Park 1997; Bozkurt 2003). Avigad *et al.* (2001) estimated that folding on Andros accounts for 40–50% of NW–SE crustal shortening.

Greenschist retrogression and associated ductile features

Greenschist deformation occurs in two steps.

The first step consists of the formation of ubiquitous sheath folds, with axes always parallel to the stretching lineation (Fig. 5). Sheath folds result from the evolution of folding of the first schistosity S_1 under intense ductile shearing. They are visible at centimetre to decametre scale and are locally observed in the core of later boudins with parallel axes. Although we have no clear observations that substantiate this conclusion, we suspect that some of the NE–SW trending boudins result from the stretching of the sheath folds.

The second step of greenschist deformation corresponds to the boudinage of the S_2 foliation.

Boudinage is a very common phenomenon on Andros. It extends over the entire area and at every observation scale (Fig. 6; see caption for more details). Although the major part of the boudinaged outcrops consists of boudins of several metres in scale of metabasites in the metapelitic matrix (Figs 6a and 7, outcrops 75, 39, 22, 17 and 2–3), boudinage commonly involves several types of materials, such as quartz or marbles (Fig. 6b and c, respectively).

Some outcrops show evidence of crystallization between boudins (metre scale: Fig. 7, outcrops 75 and 74; centimetre scale: Fig. 6d; millimetre-scale: Fig. 6e). Crystallization of albite and chlorite in the interboudin necks of outcrops 39 and 75 (Fig. 7) shows that boudinage occurred under greenschist-facies conditions. Such crystallization can be explained by the presence of stress gradients established during the development of boudins: the gradients allow the migration of the more mobile mineral elements from the surrounding areas towards the low-pressure zones; that is, the interboudin gaps and/or the ends of boudins (Price & Cosgrove 1990).

Roadcut outcrops between Gavrio and Andros show an evolution in the geometry of boudins and

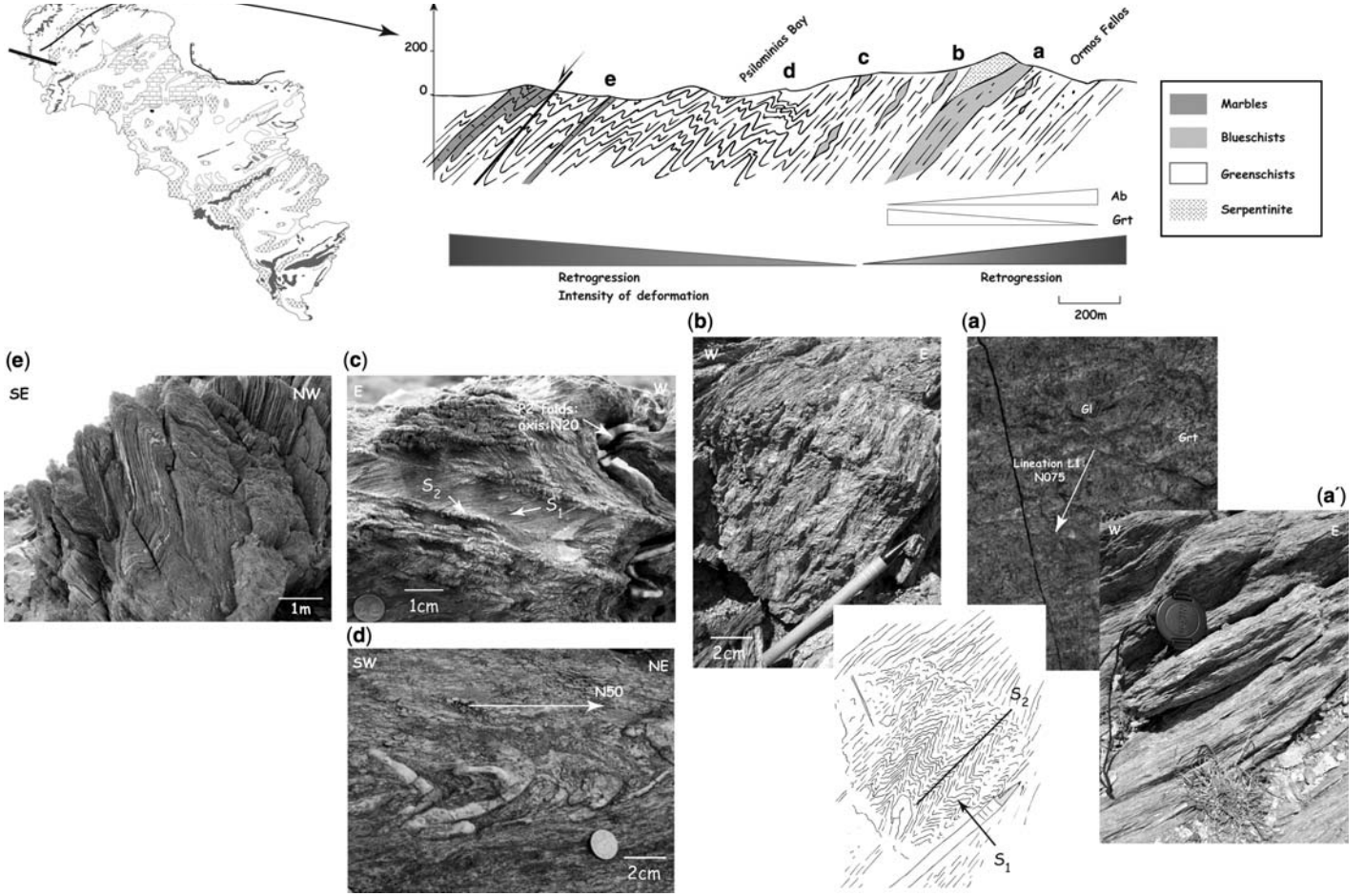

Fig. 4. Cross-section of the Makrotantalon Unit illustrating the evolution from blueschist to greenschist deformation on Andros. A gradient of retrogression is observed below and above the serpentinite body. (**a**) NE–SW-trending blueschist stretching lineation (L_1) recorded by the alignment of blue amphiboles. (**a′**) Pressure shadows on the garnets illustrating the top-to-the-NE sense of shear in blueschist facies. (**b**) Progressive formation of a greenschist S_2 foliation in the west-dipping axial crenulation plane of blueschist S_1 foliation. (**c**, **d**) Progressive curvature of P_2 fold axes (c) towards sheath folds (d) with axes parallel to the stretching lineation L_2. (**e**) Intensely foliated and folded marbles indicating the increase in intensity of deformation towards the NW.

Table 1. *Evolution of deformation from blueschist to greenschist facies along the section west of Gavrio*

Metamorphic facies, Stretching lineation	Foliation	Finite deformation	Complementary remarks
Blueschist facies			
$\mathbf{L_1}$, east–west- for NE–SW-trending (alignment of blue amphibolite needles, Fig. 4a)	$\mathbf{S_1}$	Top-to-the-NE sense of shear (asymmetry of pressure shadows on the garnets and shear bands, Fig. 4a) Open folds with a west-dipping axial-plane crenulation cleavage evolving towards S_2 (Fig. 4b and c)	Blueschists better preserved below and above serpentinite bodies
Greenschist facies			
$\mathbf{L_2}$-NE–SW-trending	$\mathbf{S_2}$	Sense of shear not clear along the section Crenulation Folding (P_2 folds, Fig. 4c) and progressive rotation of folds limbs with increasing shearing Boudinage	Increasing retrogression and intensity of shear strain when moving away from the serpentinite body (cross-section in Fig. 4) Increasing shear strain indicated by evolution of P_2 fold axes towards sheath folds (Fig. 4c and d) and intensively foliated and folded blue marbles at the top of the section (Fig. 4e)

shear bands. In the SW half of the island, boudinage leads to almost symmetrical structures when metabasites are involved (Fig. 7, left side). In the NE the geometry becomes clearly asymmetrical with NE-dipping shear bands and sigmoidal boudins indicating top-to-the-NE shear sense (Fig. 7, right side). Sequences of decametre-scale shear bands are observable in the landscape over all the capes of the northern coast (Fig. 8). They had first been interpreted by Papanikolaou (1978) as normal faults but do not show evidence of significant brittle slip. Foliation boudinage already shows a localization of non-coaxial top-to-the-NE shear in the NE half of the island.

The outcrops of Figure 9a and b illustrate the evolution from ductile to brittle structures for symmetrical (Fig. 9a) and asymmetric (Fig. 9b) boudins of metabasites embedded in a metapelitic matrix. Whatever the shape of boudins, shear bands seem to quasi-systematically localize in the necks or at the end of boudins (Fig. 9a and b; see captions for detailed descriptions), as already described on Tinos (Jolivet *et al.* 2004*a*; Mehl *et al.* 2005). The evolution towards brittle deformation is characterized by the onset of en echelon arrays of veins, whose normal shear movement is consistent with boudinage (Fig. 9a, picture A). Brittle steeply dipping planes seem to have developed on en echelon arrays of quartz veins (Fig. 9a, B; Fig. 9b, B–D), and therefore reflect the progressive and ultimate localization of normal shear. As shown in the diagrams of ductile and brittle data, the dip of shear planes increases while deformation evolves from ductile to brittle.

It is interesting to note that the metapelitic matrix of the outcrop shown in Figure 9b is

Fig. 5. Map of greenschist stretching lineation L_2 with sense of shear recorded on Andros (after Gautier 1994; Patriat 1996; this study). Stretching lineations indicate a consistent NE–SW direction of ductile stretching. Most of the photographs illustrate ubiquitous centimetre- to decimetre-scale sheath folds with NE–SW axes. They correspond to the first increment of ductile deformation. They result from the evolution of folding of S_1 under intense ductile shearing. (**a**, **b**) Sheath folds in a quartz vein included in retromorphosed metabasites of the Makrotantalon Unit. The NE–SW fold axes are parallel to the stretching lineation L_2. (**c**, **d**) Sheath folds with NE–SW axis in a boudin of metabasites. (**e**, **f**) Sheath folding of quartz veins with NE–SW axis in metabasites. Folding is sheared, as indicated by the onset of a top-to-the-NE shear band in the left part of (e). (**g**) Intense folding with NE–SW axis in metabasites of the Halkolimniona Cape. Folding can be here interpreted as resulting from a component of constriction of the deformation. (**h**) Cross-section perpendicular to a sheath fold of quartz vein in the metabasites of the Halkolimniona Cape. (**i**, **j**): Metre-scale sheath folds in metabasites of the Thiaki Cape.

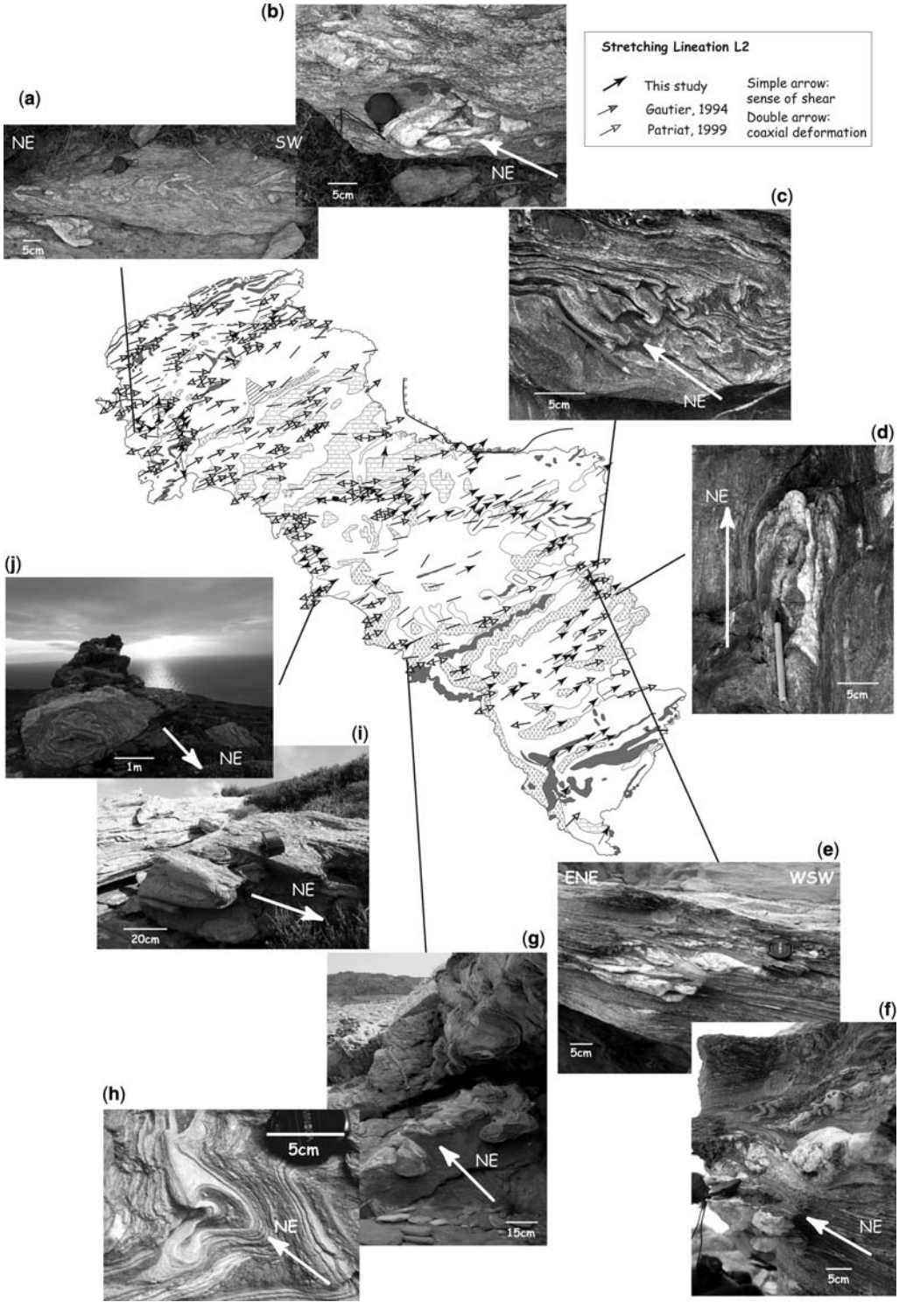
(a)
NE
SW
5cm
(b)
NE
5cm
Stretching Lineation L2
This study
Gautier, 1994
Patriat, 1999
Simple arrow: sense of shear
Double arrow: coaxial deformation
(c)
5cm
NE
(d)
NE
5cm
(e)
ENE
WSW
5cm
(f)
NE
5cm
(g)
NE
15cm
(h)
5cm
NE
(i)
NE
20cm
(j)
1m
NE

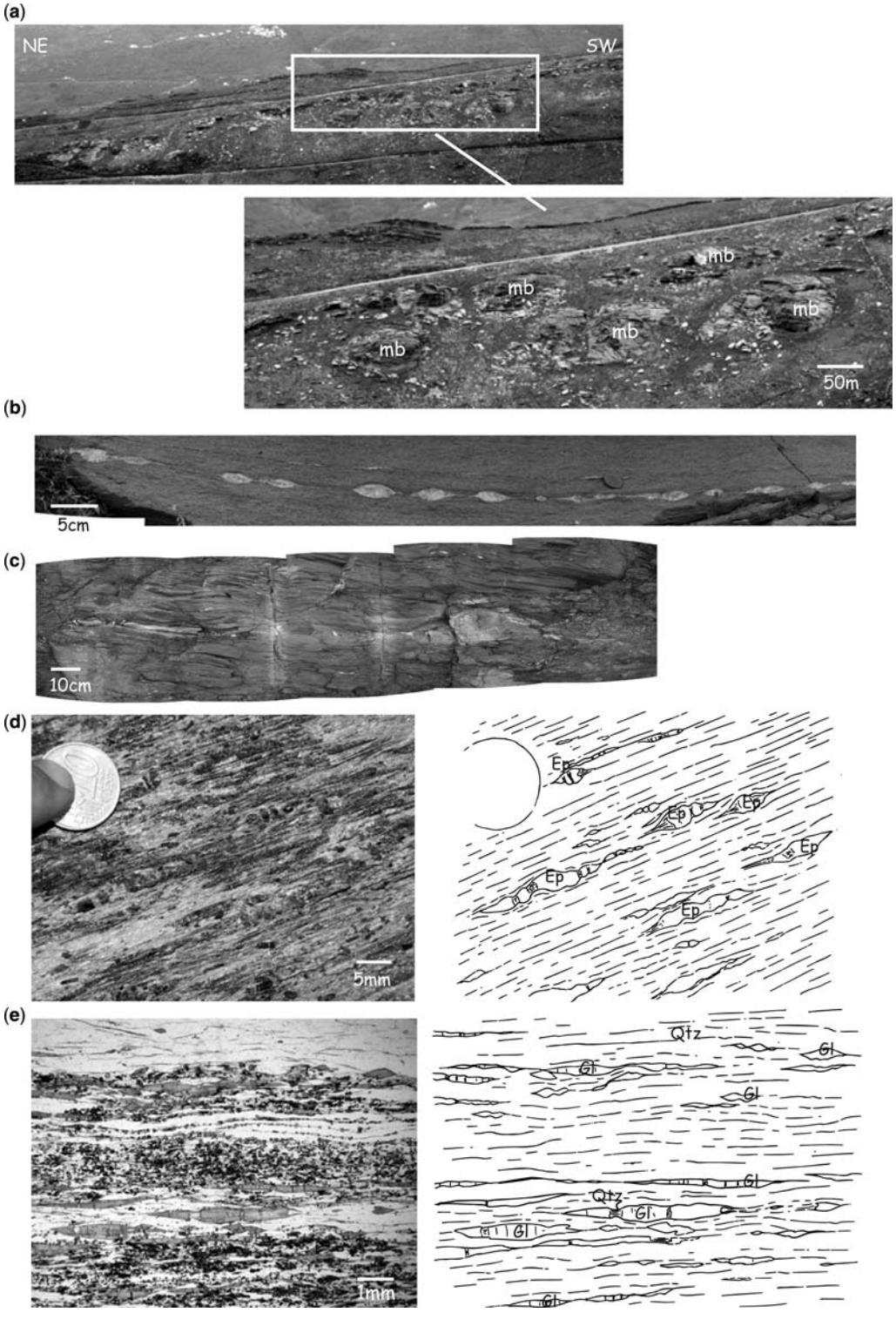
(a)
NE
SW
mb
mb
mb
mb
mb
50m
(b)
5cm
(c)
10cm
(d)
5mm
Ep
Ep
Ep
Ep
Ep
Ep
(e)
1mm
Qtz
Gl
Gl
Gl
Qtz
Gl
Gl
Gl

apparently not affected by brittle features. Localization of deformation in the metapelites is weak and is marked only by shear bands picture (A), whereas actual brittle deformation concentrates in the metabasites. This emphasizes the role of the lithological contrast in the localization process.

Semi-brittle structures

Semi-brittle shear bands can also be observed on Andros. They correspond to localized shear bands that display a latest brittle increment of extensional kinematics: foliation deviates along the plane but, contrary to a classical ductile shear band, a small offset support a late discontinuous shear movement. Some of these shear structures show slickensides which unambiguously support a brittle and normal sense of motion along the plane. They commonly correspond to planes belonging to a sequence of shear bands with increasing dip. The steeper the plane the more brittle the deformation is (Fig. 10b, A).

Brittle features

Two examples of 'brittle' outcrops are detailed in Figure 10a and b. The two outcrops are made up of an alternation of pelitic and more quartzitic beds. The quartzitic beds, being more competent than pelitic ones, are boudinaged (Fig. 10a and b, views of the entire outcrops).

The pelitic beds show the same straightening sequences as the outcrops of Figure 9a and b (Fig. 10b, picture A). The main brittle features observed here correspond to joints, veins and fault planes. Displacements of beds, striations on fault planes and rotations of en echelon arrays of veins argue for the extensional nature of deformation. Only major faults cut across the entire outcrops (Fig. 10a, picture B).

Conjugate patterns of normal faults, veins and joints are well expressed in the two outcrops. Although one plane cuts across the entire outcrop of Figure 10a, most conjugate sets of faults are concentrated in the quartzitic layers (Fig. 10a, A). When focusing on the northernmost part of the outcrop, we can see that joints concentrate in quartzitic beds (Fig. 10a, B). The same conclusion can be reached concerning the veins of the outcrop shown in Figure 10b: en echelon arrays of veins are concentrated in the light beds (Fig. 10b, panorama and C). This feature is particularly obvious in Figure 10b, picture B: veins clearly stop at the interface of the two beds.

En echelon arrays of veins and joints define rough planes whose orientation, dip and kinematics are comparable and consistent with classical conjugate sets of normal faults. Sometimes, these en echelon structures evolve toward true normal faults. This evolution is statistically more common for NE-dipping planes. However, the brittle planes do not propagate in the pelitic beds: structures flatten in the dark beds (Fig. 10a, C), and they seem to be relayed by shear bands in these pelitic beds (Fig. 10b, B).

Measurements of directions and dips of mesoscale striated faults, postfolial joints and veins were carried out all over the island. The most prominent fault sets trend NW–SE. Whatever the lithology, en echelon veins and normal faults clearly support extensional kinematics. Poles of veins and joints, together with orientation of faults and slip vectors on fault planes, consistently indicate a NE–SW direction of extension (Fig. 11). Reconstruction of stress regimes was carried out from fault slip data. This reconstruction was necessary to determine whether or not stress axes underwent a significant rotation in the latest stage of brittle deformation. Our fault slip data were collected on late, outcrop-scale faults displaying small offsets and a large scatter in attitudes, and cutting generally through the ductile rock fabrics (foliation and shear bands), and away from the detachment zone. Thus palaeostress reconstructions reported in this paper fulfil the assumptions of stress homogeneity and low-finite strain, which can be approximated by nearly coaxial conditions, and therefore probably yield the regional palaeostresses of interest. The *a posteriori* consistency of the stress regimes derived from both the inversion of striated faults and the statistical analysis of vein patterns, from one site to another, in spite of significant lithological variations (metabasites, metapelites, quartzitic beds), supports the reliability of the results. The aim of our stress analysis is, therefore, to

Fig. 6. Boudinage on Andros. The locations of the outcrops are shown on the map of Figure 2. Boudinage occurs at every scale and involves several types of materials over the whole island. (**a**) Outcrop 04; several-metre-scale boudins of metabasites that are visible in the landscape (mb, metabasites; mp, metapelites). (**b**) Outcrop 44; decimetre-scale synfolial quartz veins regularly boudinaged in the metapelitic matrix. (**c**) Outcrop 07; decimetre-scale boudinage also involves layers of marble in the metapelitic matrix. (**d**) Centimetre-scale boudinage of epidotes (Ep) in the matrix of Thiaki Cape. In this case, inter-boudins are filled with quartz precipitated in irregular voids. The schistosity is deflected around boudins: micas follow the shape of boudinaged epidotes. (**e**) Thiaki Cape; thin section illustrating millimetre-scale boudinage. This is an example of syn-greenschist boudinage of glaucophanes (gl) (the foliation is horizontal in this cross-section) and growth of quartz (Qtz) in the inter-boudins or at the end of boudins. Small-scale boudinage is coeval with penetrative stretching and intense ductile shearing.

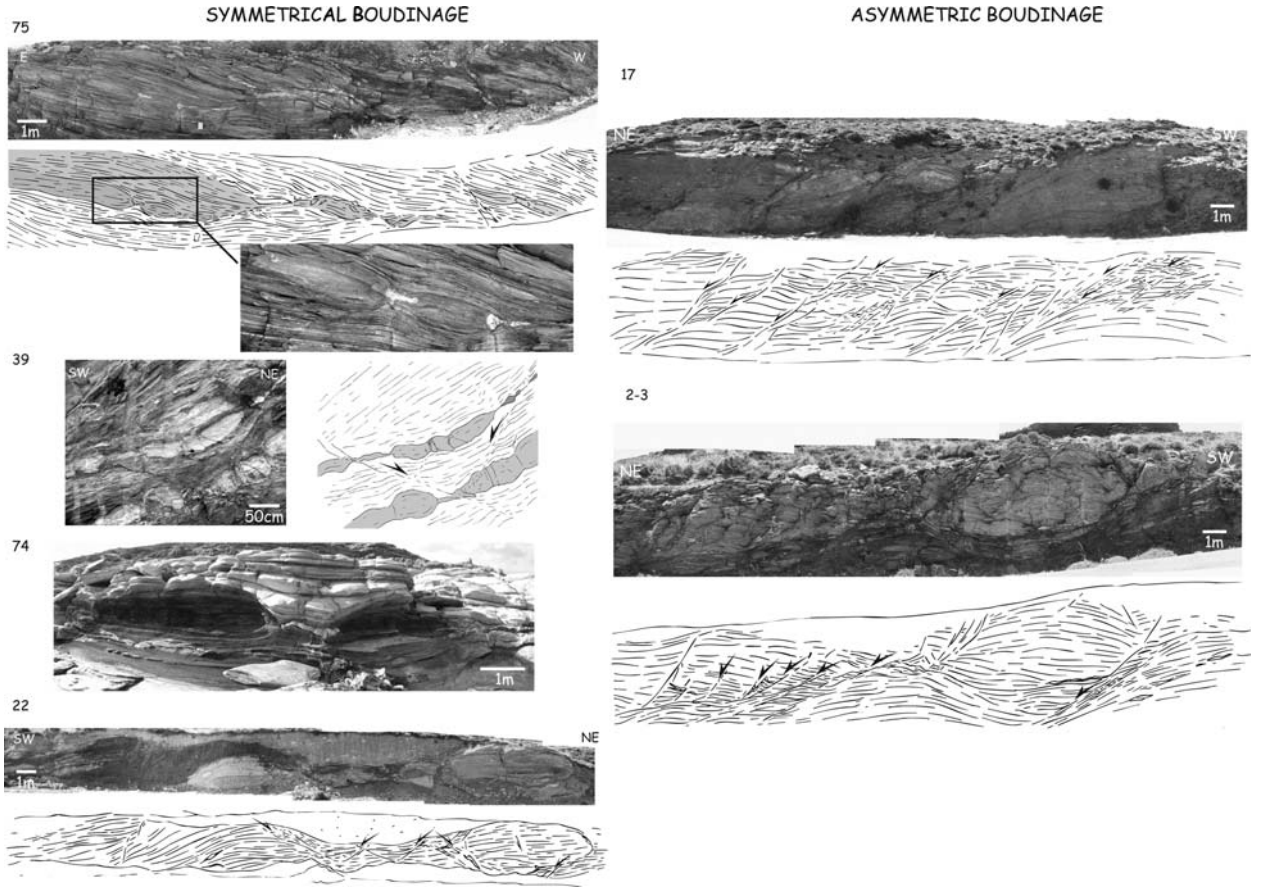

Fig. 7. Boudinage as the initial factor of localization of deformation. The locations of outcrops in this figure are shown in Figure 2. Outcrop 75: symmetrical boudinage in a metabasite matrix. Inter-boudin gaps and the ends of boudins are filled with quartz veins. Outcrop 39: Centimetre-scale symmetrical boudin of metabasite in a metapelitic matrix, Thiaki Cape. Conjugate shear bands develop in the neck between boudins. Outcrop 74: Metre-scale 'shadows' of symmetrical boudins in marbles of the southern cape of the island. Inter-boudin gaps are filled with quartz veins. Outcrop 22: several-metre-scale boudins of metabasite embedded in a metapelitic matrix in the central part of the island. Conjugate shear bands localize in the neck between boudins. Outcrop 17: asymmetric boudins of metapelite in a metapelitic matrix. Shear bands localize at the end of boudins and dip systematically towards NE. Outcrop 2 − 3: several-metre-scale boudins of metabasite in a metapelitic matrix. NE-dipping shear bands localize at the end or in the neck of the boudins. Boudins evolve from a symmetrical shape (left-hand side of the figure) in the southern part of the island towards an asymmetric one in the north-eastern part (right-hand side of the figure). The evolution of shape is interpreted is related to an increase in the intensity of shear deformation from SW to NE.

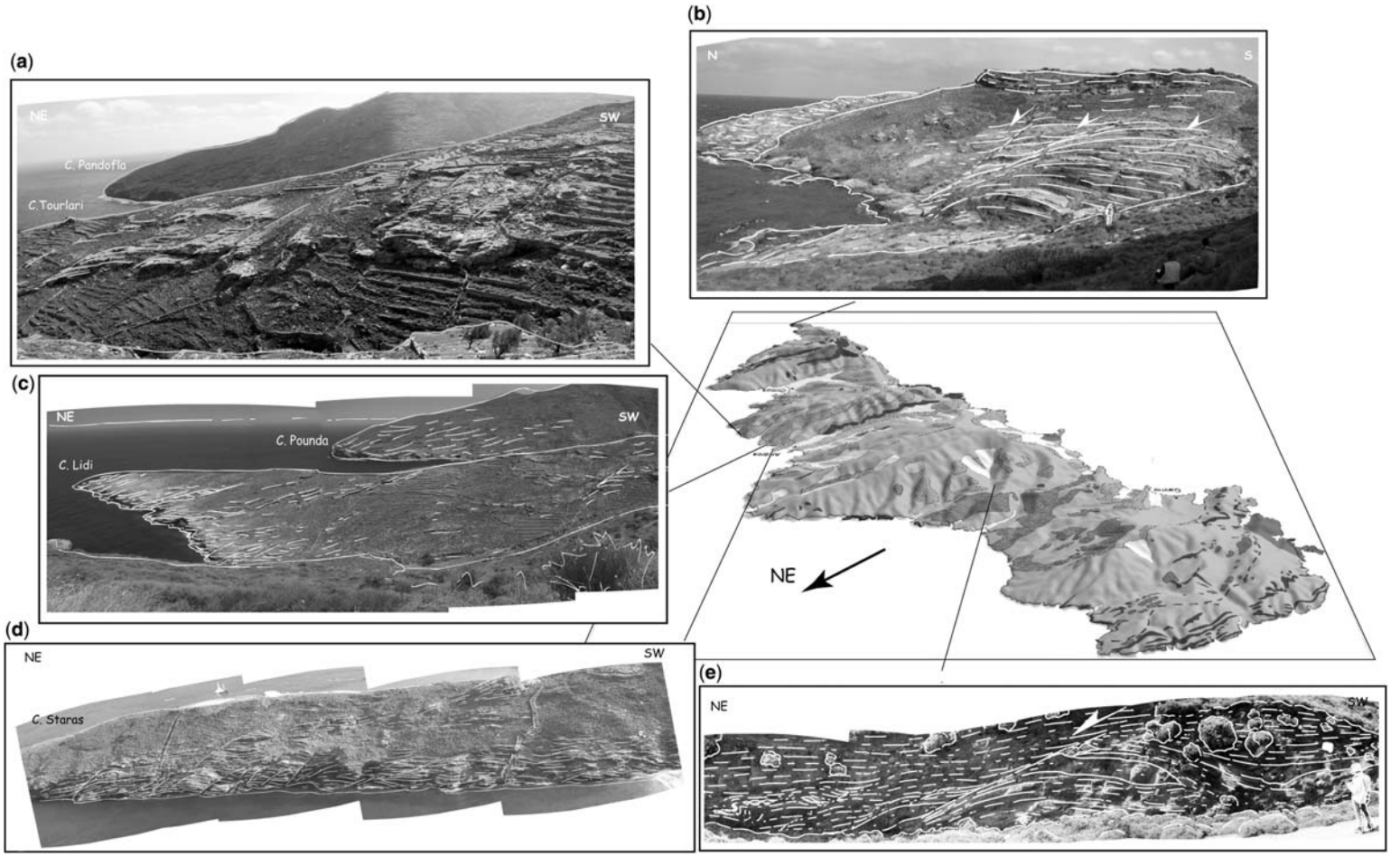

Fig. 8. Structural landscapes illustrating decametre-scale shear bands on the northeastern capes of Andros (for location, see Fig. 2). (**a**) NE-dipping, regularly spaced shear bands on the Tourlari Cape. (**b**) Several-metre-scale, NE-dipping shear band affecting the marbles of the southern cape of the island. (**c**, **d**): Several-metres-scale shear bands on the Lidi and Staras Capes. (**e**) NE-dipping shear band affecting the metapelites of the central part of the island.

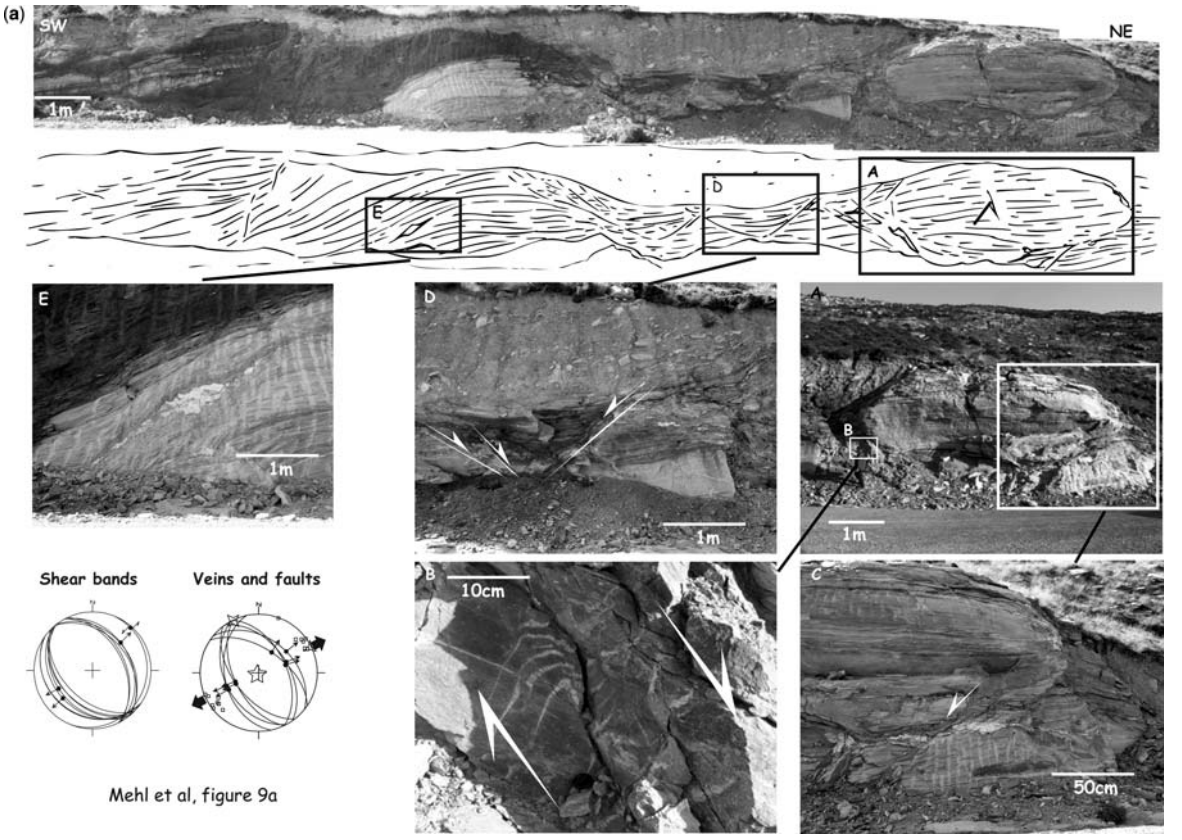

Fig. 9. (**a**) Evolution of deformation from ductile to brittle. The outcrop shows two symmetrical boudins of metabasites embedded in a metapelitic matrix. The ends of boudins show evidence of brittle–ductile to brittle deformation. (**A**) The SW end of the westernmost boudin showing an en echelon array of quartz veins in the metabasite. (**B**) This en echelon pattern testifies to a local normal shear movement that is kinematically consistent with boudinage. The ultimate step of localization consists of the development of an actual normal fault cutting through the en echelon system. (**C**) The NE end of the boudin shows a brittle normal steeply dipping plane. (**D**) Symmetrical patterns of shear bands can be observed in the inter-boudin gaps. As shown in the diagrams of ductile and brittle data, the dip of shear planes increases while deformation evolves from ductile to brittle. (**E**) Focus on a metre-scale boudin of quartz embedded in the pluri-metre-scale boudin of metabasites.

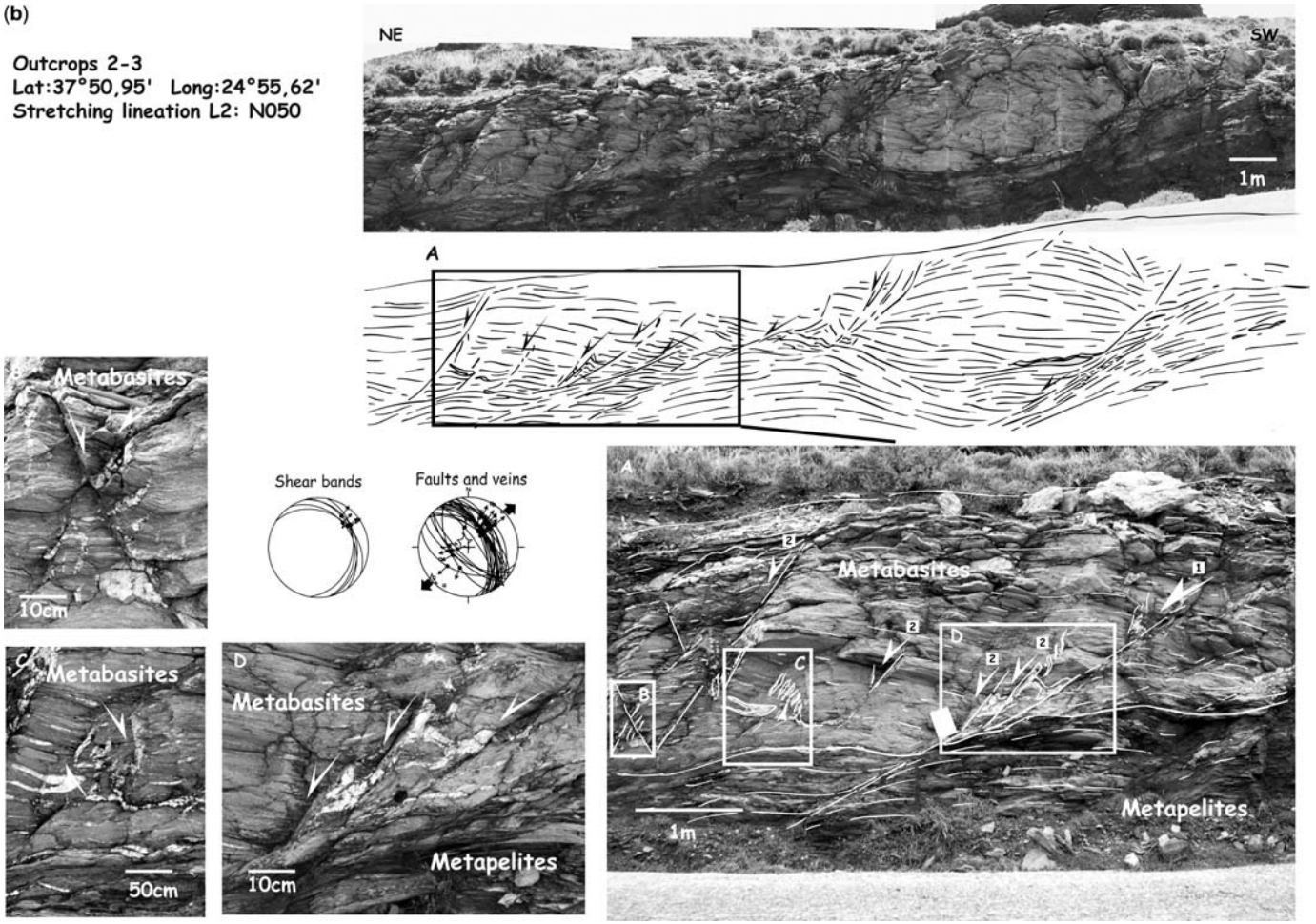

Fig. 9. (*Continued*) (**b**) Evolution of deformation from ductile to brittle around an asymmetric boudin of metabasite embedded in a metapelitic matrix. The metapelitic matrix is apparently not affected by brittle features. Localization of deformation in the metapelites is weak and is marked only by shear bands, whereas actual brittle deformation concentrates in the metabasites. (**A**) NE-dipping shear bands preferentially localize at the end of boudins. (**B**, **C**) En echelon arrays of quartz veins on which brittle planes develop. Brittle planes sometimes display conjugate patterns. (**D**) Steeply dipping brittle planes connected to ductile shear bands. Onset of brittle deformation is shown by onset of en echelon arrays of veins and progressive steepening of ductile structures, as illustrated by the diagram of ductile and brittle data.

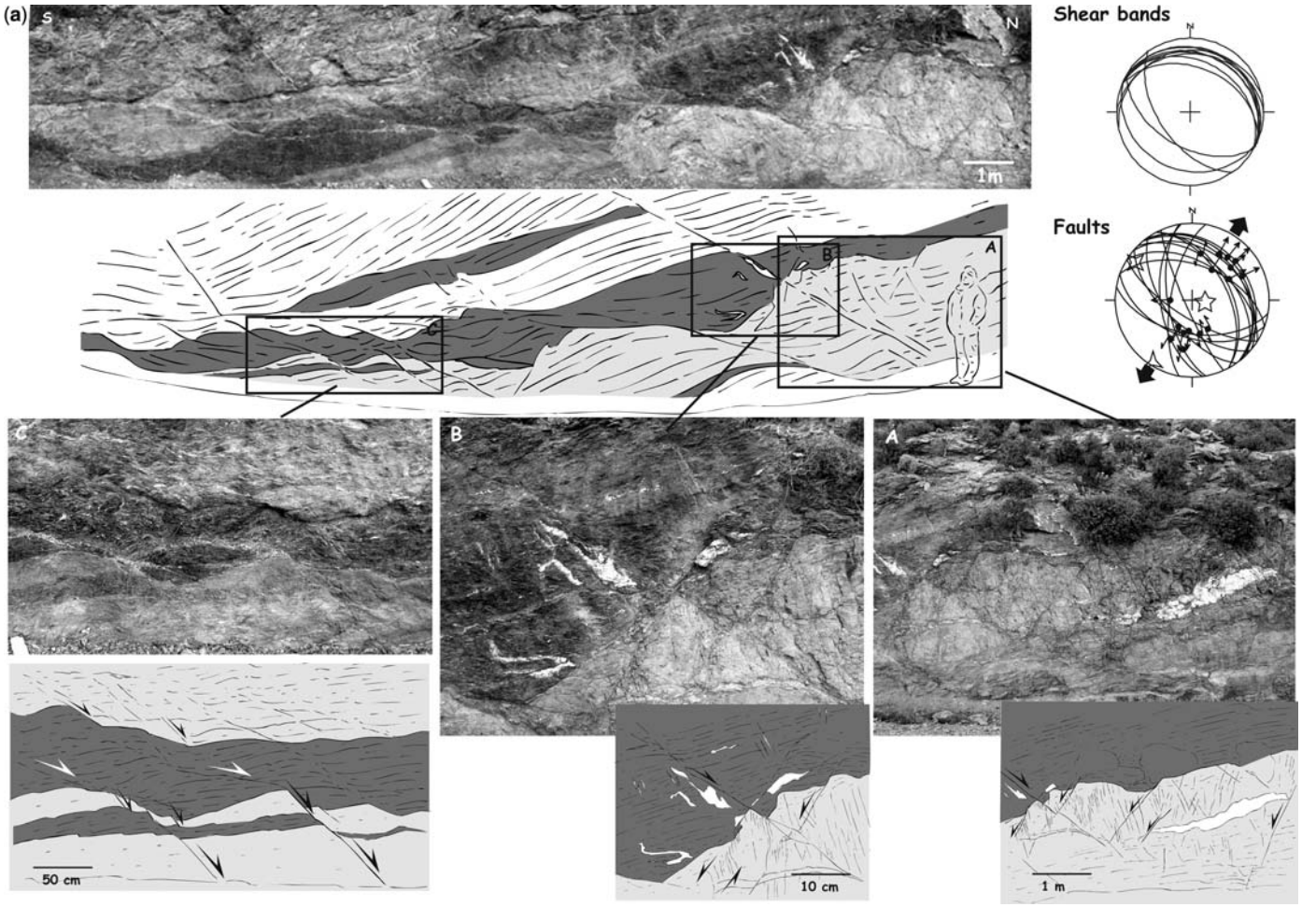

Fig. 10. Rheology as a key parametre in the localization process. Alternation of metapelites (dark grey) and quartzitic (light grey) beds. Quartzitic beds are more competent than metapelites and are boudinaged. Brittle features (en echelon arrays of veins, steeply dipping faults) preferentially localize in quartzitic beds (**a**, **A**–**C**; **b**, **B** and **C**) whereas shear bands are better preserved in metapelitic beds (**a**, **C**; **b**, **B**).

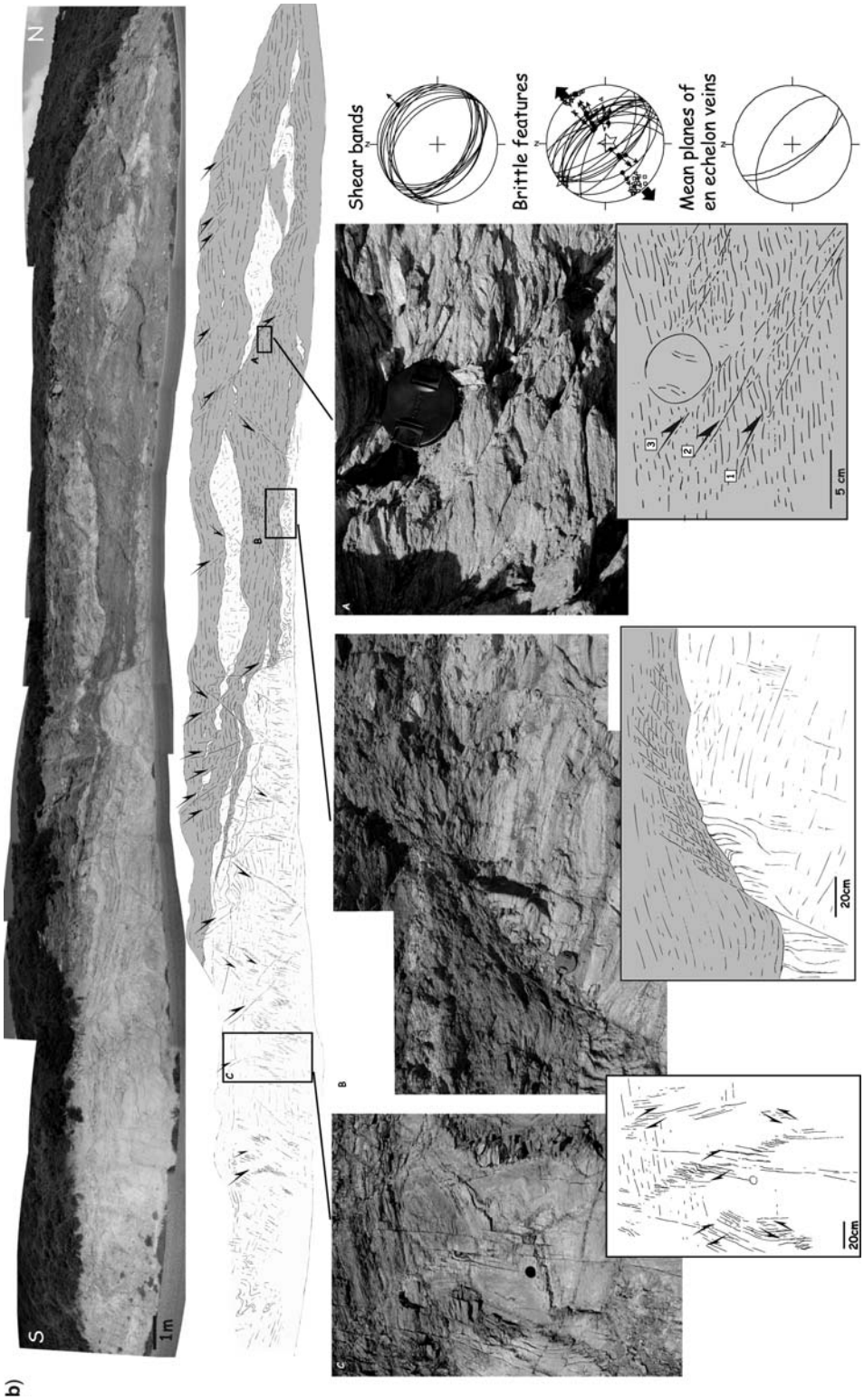

Fig. 10b. *(Continued)*

derive the orientation of the maximum principal stress σ1, which will be compared with the attitude of veins. Stress tensors were calculated using a direct analytical inversion method (Angelier 1990), assuming that the slip direction in any given plane is parallel to the direction of maximum resolved shear stress of a large-scale homogeneous stress tensor (Wallace 1951; Bott 1959). For the studied outcrops, all data were retained when computing a single tectonic event. A reduced stress tensor is obtained; that is, the orientation of the principal stress axes σ_1, σ_2 and σ_3 ($\sigma_1 \geq \sigma_2 \geq \sigma_3$, compression positive) and a scalar invariant ϕ characterizing the shape of the stress ellipsoid:

$$\phi = (\sigma_2 - \sigma_3)/(\sigma_1 - \sigma_3),\ 0 \leq \phi \leq 1.$$

Inversion minimizes the misfit of the predicted shear and observed slip within the fault plane. Where the stress axes are computed from well-defined conjugate fault sets, as at most sites on Andros, the uncertainties in their orientation are lower than 10°. The good agreement between the stress axes computed from striated faults and the orientation of veins measured at the same sites confirms that the results obtained are reliable and accurate.

Results are presented using Schmidt's lower hemisphere projection (Fig. 11); orientations and dips of principal stress axes are reported in Table 2, together with the values of the stress ellipsoid shape ratio ϕ and estimators of the quality of the numerical calculation of the tensor. At most sites where the foliation is subhorizontal or displays a gentle dip, the computed stress axes σ_2 and σ_3 are horizontal or gently dipping and the σ_1 axis is subvertical, despite the variations between lithologies. This subvertical orientation is consistent with the vertical patterns of veins often associated with normal faults and characterizes an extensional tectonic regime. A consistent NE–SW direction of brittle extension is therefore recognized over the whole island. One outcrop is an exception to the rule, with a computed reverse-type tensor (southern coast of the island, Fig. 12a). For all the outcrops, it is noticeable that the maximum stress axis σ_1 is always nearly perpendicular to the foliation whatever its dip.

Some outcrops have been detailed in Figure 12. The brittle deformation of the outcrops shown in Figure 12a and b is characterized by veins and conjugate patterns of brittle faults. In the first outcrop, the foliation is dipping 71° west and indicators on fault planes and displacements of the beds along the faults indicate a reverse sense of motion. In the second outcrop, the foliation is dipping 42° west. Slip indicators and displacement of quartz veins show a normal sense of motion. Veins are perpendicular to the foliation and are bisectors of the acute angle between faults. In the two cases, the structures seem to have been tilted by the value by the foliation dip. When tilting the foliation around its local strike back to horizontal, 'unfolding' (Fig. 12b and c, second diagrams), a consistent NE direction for brittle extension is obtained, the stress axes becoming similar in trend to those determined at sites with subhorizontal foliation. This observation can be made even at sites where the dip of foliation remained gentle (Fig. 13). These results strongly suggest that all brittle structures of the island formed under a vertical maximum stress axis σ_1 and with an almost flat-lying foliation. Both the foliation and the brittle fault systems were therefore tilted later (see below).

Except at two sites where the values are low (0.14), the ϕ values calculated are in the range of 0.21–0.47, suggesting a generally well-defined true triaxial stress regime throughout the island.

Interpretation of field data and discussion: evolution of structures from ductile to brittle

Stretching lineation and stress tensors deduced from the inversion of fault slip data indicate a consistent NE–SW extension during ductile and brittle deformation. This leads us to conclude that there was a continuum of kinematics from ductile to brittle. We now discuss how brittle deformation is superimposed on ductile deformation during extension and the exhumation of the Lower Unit.

At the outcrop scale

Initial localization of ductile shear bands: the role of boudinage. In the presence of boudins, of whatever the scale and type (symmetrical or asymmetric), shear bands often nucleate at the end or in the necks between boudins, as already observed on Tinos (Jolivet *et al.* 2004*a*; Mehl *et al.* 2005): we can thus confirm that boudinage (and more generally lithological heterogeneities) is an efficient localizing factor of ductile and brittle deformation (Fig. 9a and b). Ductile shear bands, observed at decametre to millimetre scale all over the island, evolve, as do boudins, from symmetrical patterns on the southern coast towards asymmetric ones when approaching the detachment.

Onset of brittle deformation. The existence of semi-brittle shear bands shows the way in which brittle structures are superimposed on ductile ones. When brittle slip occurs along previous ductile shear planes in a direction strictly parallel to the stretching lineation, this superimposition

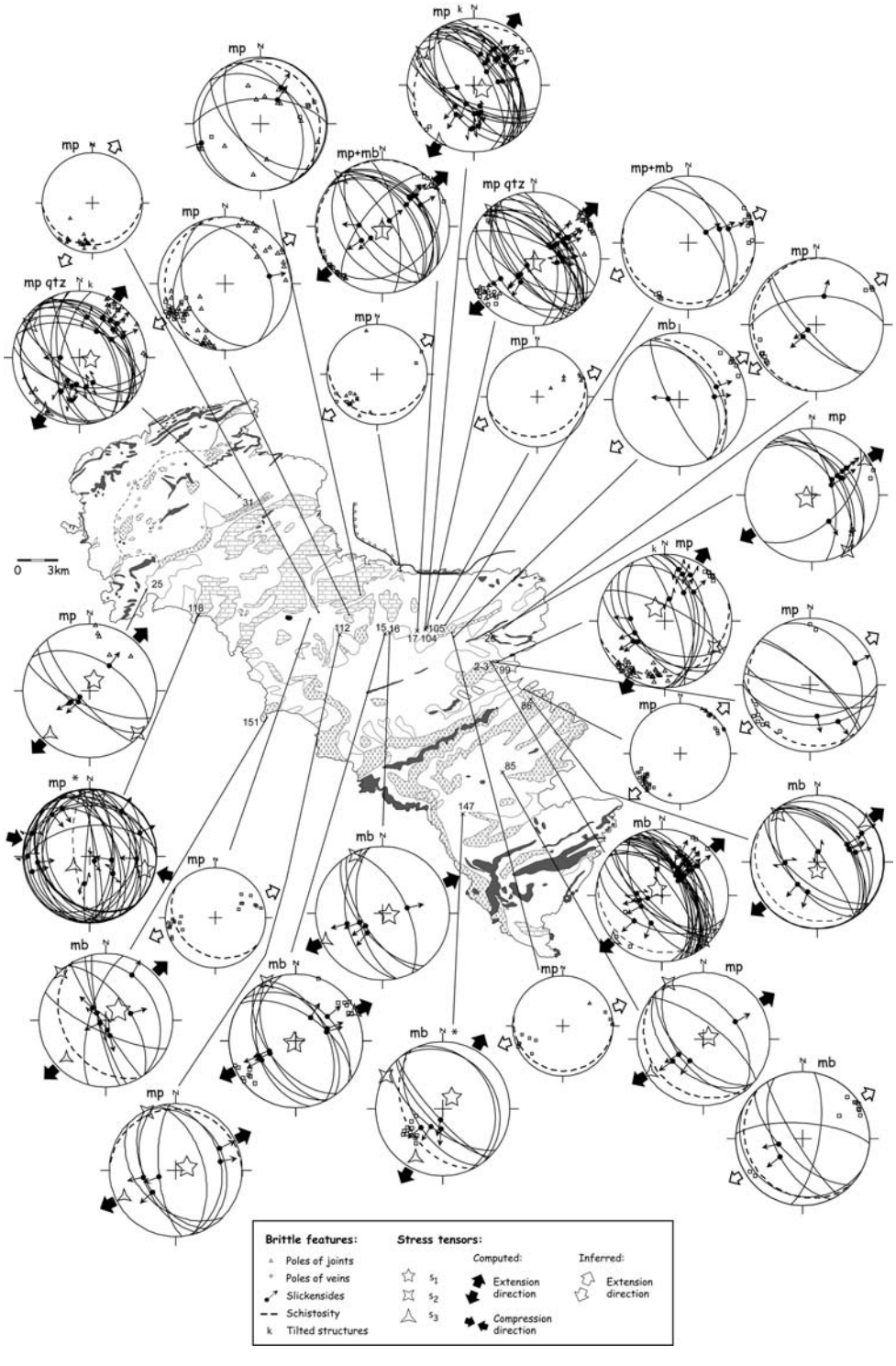

Fig. 11. Schmidt's lower hemisphere equal-area projection of brittle structures of Andros. mp, measurements made in metapelites; mb, measurements made in metabasites. The foliation is indicated by a dashed line. The computed and inferred brittle extension directions are in good agreement with ductile stretching (stretching lineation map of Figure 4).

Table 2. *Trends and plunges of axes of stress tensors deduced from the direct inversion of orientation and striae of faults*

Outcrop	Lithology	Number of fault planes	Strike/dip of foliation	σ_1	σ_2	σ_3	$\phi = (\sigma_2 - \sigma_3)/(\sigma_1 - \sigma_3)$	Quality estimator
15	**Metabasites**	8	–	222/87	334/01	064/03	0.29	A
16	**Metabasites**	5	–	104/82	335/05	244/06	0.32	A–B
17	**Metapelites** + metabasites	9	040/02	186/85	320/04	050/04	0.41	A
25	Metapelites	4	–	021/76	131/05	223/13	0.30	B–C
26		7	–	244/83	148/01	057/07	0.27	B
2–3	**Metabasites**	27	290/16	321/80	138/10	228/01	0.37	A
31	**Quartzitic metapelites**	16	–	097/71	297/18	205/06	0.46	A
85	Metapelites	4	315/17	068/83	328/01	238/07	0.28	B–C
86	**Metabasites**	9	304/14	181/79	320/08	051/07	0.52	A
99	Metapelites	10	254/18	324/71	118/17	210/08	0.30	B
104	Metapelites	25	050/18	116/80	302/10	212/01	0.37	A
105	**Quartzitic metapelites**	20	–	152/82	323/08	053/01	0.31	A
112	Metapelites	5	095/09	076/76	334/03	243/14	0.14	A–B
118*	Metapelites	13	354/71	104/17	009/15	239/67		A–B
				195/56	**347/31**	**085/13**	0.54	
147*	**Metabasites**	8	332/42	038/72	300/03	209/18		A–B
				270/75	**122/13**	**030/08**	0.40	
151	**Metabasites**	7	330/5	051/71	317/02	226/19	0.14	C

A quality estimator (A–C) has been attributed to each numerical result, based on the number and variety of attitudes of faults and on an intra-algorithm estimator accounting for the mean deviation between the computed shear stresses and the actual measured striations. Stress axes are given in their current attitude. Back-tilted stress axes are shown in bold.
Outcrops shown in Figure 14 where structures and foliation have been tilted by a significant amount.

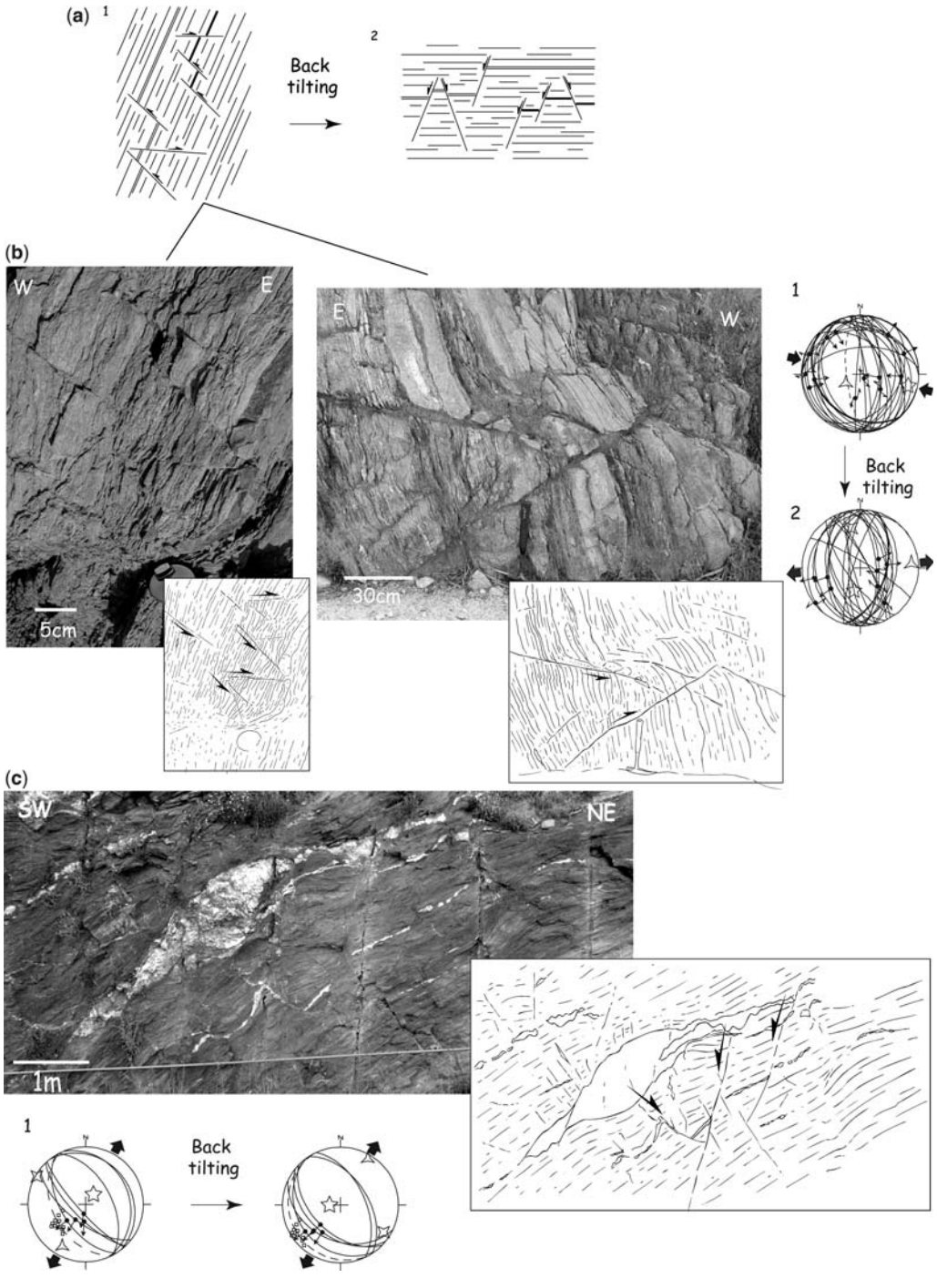

Fig. 12. (**a**) Principle of back-tilting of brittle structures. (**b**, **c**) Examples of tilted structures. (**B**, outcrop 118; **C**, outcrop 147) and associated Schmidt's diagrams showing the present attitude and the attitude of back-tilted fracture sets and foliation. It should be noted that after back-tilting, computed tensors correspond to a consistent NE–SW direction of brittle extension and a nearly vertical position of σ_1, in agreement with the vertical attitude of veins.

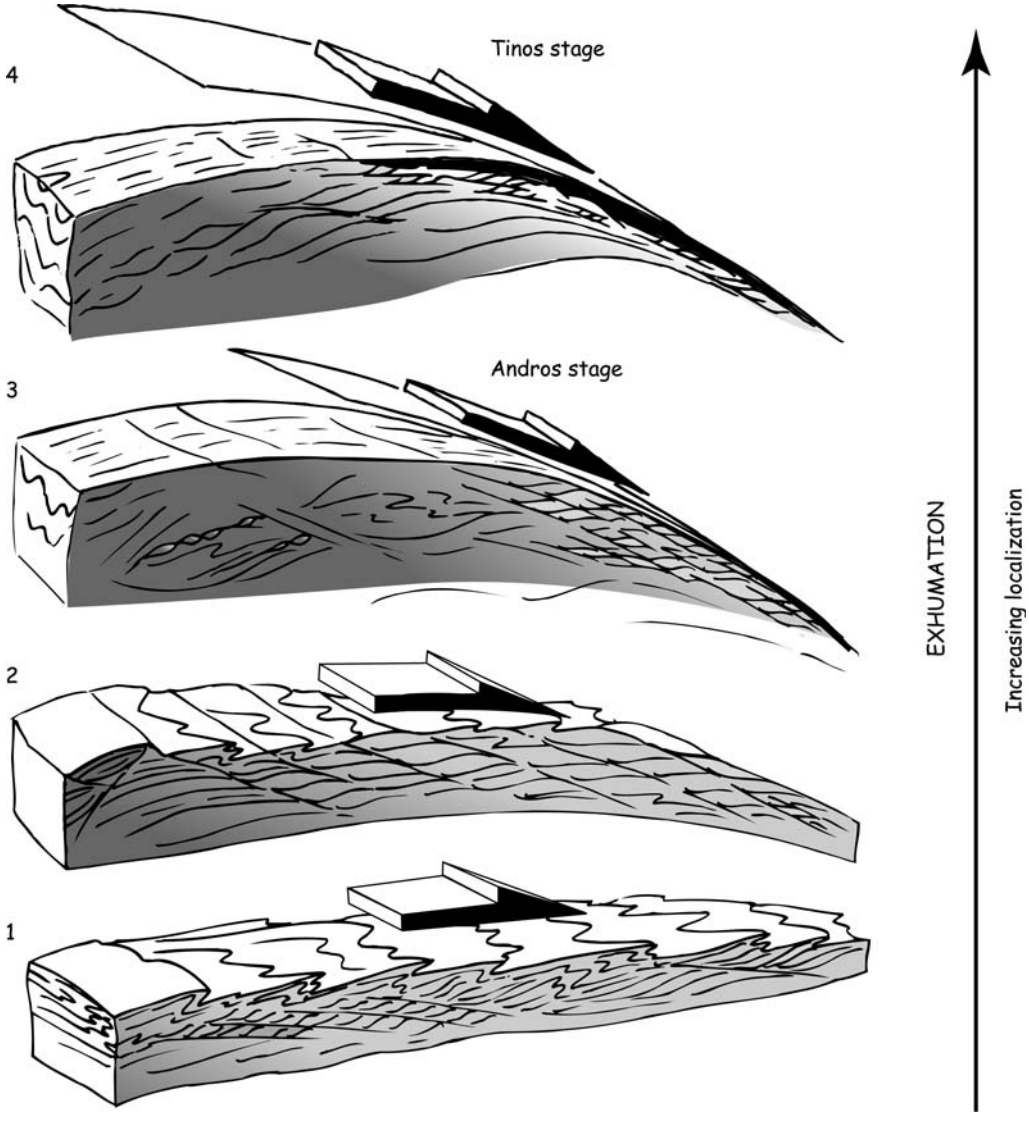

Fig. 13. Conceptual four-step scenario of evolution of deformation from ductile to brittle. (1) Formation of ubiquitous greenschist foliation under high finite strain and non-coaxial flow, as indicated by onset of sheath folds. (2) Boudinage of the foliation and onset of spatial distribution between coaxial and non-coaxial flow. Shear bands localize in interboudin necks. (3) Localization of non-coaxial flow in the northeastern part of the island. (4) Evolution of shear bands from semi-brittle to brittle structures. Deformation localizes in the NE, below the contact with the Upper Unit, to finally form the detachment itself. A new stage in the exhumation process has been proposed for Andros compared with a previous study (Mehl *et al.* 2005) (stage 3), which allows us to propose a complete section of an extending continental crust.

corresponds to a kind of 'reactivation' of a precursory ductile anisotropy. 'Reactivation' commonly refers to sliding along a pre-existing discontinuity; instead, we mean here that the discontinuous brittle slip is 'prepared' by ultimate localization of shear within a precursory shear band under a continuous extensional kinematics. Only the more steeply dipping shear bands show reactivation as brittle faults.

Numerous outcrops of the island show a succession of progressively steepening shear planes. The early shallow planes are almost parallel to the

underlying ductile shear zones and we can observe an increasingly brittle behaviour, with first a slight bending of the foliation plane on either side of the semi-brittle shear zone and then a clear offset in a sense compatible with the ductile shear. Predominant brittle normal planes dip to the NE but conjugate planes with slip senses toward the SW are also observed on the same outcrop (Figs 9b and 10b). The ultimate step of evolution corresponds to steeply dipping fault planes showing calcite steps and slickenside lineations. Such an evolution can be explained as follows: during their return to the surface, rocks underwent a decrease in temperature and pressure that induces an evolution towards a more competent rheology (i.e. an increase in the internal friction angle). The increase in the internal friction angle supposes a decrease in the angle between the plane and σ_1, σ_1 remained vertical at least during the late brittle evolution of Andros, as indicated by vertical veins and σ_1 axes computed from faults at sites where foliation is subhorizontal and after back-tilting of vein and fault sets at sites where foliation is steeply dipping. Considering a subvertical σ_1, it is not surprising that the more brittle the regime, the more important is the dip of features. A progressive straightening of structures is a classical evolution from ductile to brittle.

'Reactivation' is not the only way for brittle features to develop. Some of them are newly formed. Joints and veins are often associated in en echelon arrays, already described by Papanikolaou (1978). En echelon arrays of veins and joints define shear zones whose orientation and dip are comparable with classical conjugate sets of normal faults. They occur in the more competent layers of the studied outcrops; that is, in the boudins of metabasites (Fig. 9a) and in quartzitic layers of the pelitic outcrops (Fig. 10a and b). NE-dipping planes are commonly better expressed than SW-dipping ones; that is, en echelon arrays associated with a SW dip are less numerous. En echelon arrays of veins and joints seem to play an important role on Andros in the progressive localization toward brittle deformation. They are interpreted here as the earliest step of localization before the steeply dipping normal patterns of faults initiate.

Scenario of localization process. Field observations allow us to propose a first-order scenario of evolution of deformation from ductile to brittle, under a continuous kinematic evolution. Primary localization of ductile deformation is closely linked to boudinage and the evolution to brittle deformation is marked by progressive straightening of structures and the onset of en echelon arrays of veins or joints. The ultimate step of localization consists in sliding across the en echelon patterns and the onset of actual brittle steeply dipping planes generally displaying conjugate patterns. Exhumation is thus accompanied by an increase in localization of deformation from ductile to brittle, pervasive normal faults reflecting the ultimate step of localization.

Role of the lithological contrast in the localization process. The preferred occurrence of brittle features in the more competent lithologies indicates the control of the rheology on the localization process. The importance of the rheological contrast has already been emphasized in the description of the earliest increments of localization of deformation. By considering boudinage as the initial localizing factor of ductile deformation, we implicitly assume a dominant role of lithological contrast in the first stage of localization. This control is always very important during the last brittle increments of deformation: brittle behaviour is preferentially observed (and presumably appeared earlier) in more competent layers (metabasites and quartzitic layers). Although the first-order scenario we propose is in good agreement with the sequential evolution of structures from ductile to brittle, rheological behaviour of materials appears as a key point in the description and understanding of the localization process. Rheological heterogeneities probably have a dominant affect on the depth at which the structures initially localize during their return to the surface.

At the island scale

The scenario of evolution of deformation from ductile to brittle discussed above at the outcrop scale also applies at the scale of the island, taking into account the distribution of ductile and brittle deformation across Andros. A conceptual scheme of time and space evolution of structures at island scale is proposed in Figure 13, steps 1–3, for Andros. Field observations show a progressive concentration of non-coaxial deformation along the NE coast. Post-HP deformation begins with the formation of a greenschist foliation, present all over the island; that is, associated with evidence for high finite strain rates and non-coaxial flow such as sheath folds. The foliation is further boudinaged. At this stage a spatial distribution of coaxial and non-coaxial deformation is already observed, with symmetrical boudins in the SW and asymmetrical ones in the NE. The sense of shear is consistently toward the NE in the NE part. There is thus localization of non-coaxial flow in the NE at the scale of the island. The formation of boudins is accompanied by the formation of shear bands in interboudin necks. These shear bands are symmetrical in the SW and asymmetrical with a consistent top-to-the-NE shear sense in the NE. Within

metapelites a component of non-coaxial strain is always present. During exhumation, when shear bands evolve progressively to semi-brittle then brittle structures, deformation tends to localize in the NE below the contact with the upper plate and finally along the detachment itself. During this evolution, minor additional contacts also concentrate the shear, such as the base of some marble units, as in Paleokastro. The progressive concentration of deformation in a narrow zone explains the better preservation of HP parageneses and of early ductile structures on the southwestern coast of the island. The ultimate step of localization could correspond to the onset of the flat detachment himself; that is, a planar discontinuity that may have experienced cataclastic flow (compare the reddish breccia) before the last increment of brittle sliding. The gentle dome of foliation encompassing the whole island thus can be seen as a crustal-scale boudin with localization of a crustal-scale shear zone and later of a shallow-dipping fault at one extremity.

Doming, interpreted here as crustal-scale boudinage, is thus primarily a syn- to post-greenschist feature. Similar observations were recently made in the Betic Cordillera, where the formation of crustal-scale domes (Sierra Nevada, Sierra de Los Filabres, Sierra Alhamilla) also starts to be recorded by greenschist structures during exhumation (Augier *et al.* 2005). Folding affects greenschist facies on Tinos as well as on Andros and is interpreted to have occurred near (or above?) the brittle–ductile transition (Avigad *et al.* 2001). This means that folding is, like doming, a syn- to post-greenschist feature.

Numerous studied outcrops show palaeostress tensors computed from the measurement of brittle features with stress axes slightly tilted. All the brittle structures of Andros probably formed under a vertical maximum stress axis σ_1, but have been locally tilted in a late stage of deformation. This supposes that the schistosity was nearly flat before the onset of brittle structures. Tilting could be attributed to doming as well as to large-scale open folds described by Papanikolaou (1978) and Avigad *et al.* (2001), probably to a combination of both, but how can we explain a flat schistosity at the time brittle structures developed? Two hypotheses can be made. (1) Early ductile doming developed with a gentle curvature on Andros and ductile folding remained limited before brittle deformation occurred, so the schistosity remained nearly flat at this stage on most of the island. Doming and folding were thus mostly achieved after the onset of the first brittle structures. (2) Despite a first-order continuous evolution from ductile to brittle, local rheological contrasts or strain rate variations could have led to alternation of ductile and brittle behaviour across the transition, leading, for instance, to brittle deformation within metabasites while the pelitic matrix was still deforming more or less ductilely by folding. The two explanations do not contradict each other. Doming and large-scale open folding could have remained limited at the time of occurrence of the first increment of brittle deformation, and have later led to tilting of brittle structures developed mainly in competent material. In addition, folding, which is related to NW–SE shortening perpendicular to extension, certainly initiated in ductile conditions but possibly ended in the brittle field; this could be in good agreement with the component of NW–SE constriction recorded on Tinos and marked by late crenulation and brittle strike-slip faults (Mehl *et al.* 2005).

Comparison with Tinos

Tinos and Andros belong to the same crustal block of the Aegean Sea. They both correspond to b-type metamorphic domes; that is, domes elongated perpendicular to the main stretching direction (Jolivet *et al.* 2004*a*). Two metamorphic units are exposed on the islands and are separated by a reddish brecciated zone and a detachment (Fig. 14). The Upper Unit crops out on the northern coast of the two islands but occurs on Tinos over a larger area. The lithologies of the two Lower Units are comparable, with alternating metapelites, marble horizons and metabasites, the latter two being boudinaged into the less competent matrix of metapelites. Boudins are more numerous on Andros because the finite deformation is less severe, but are also observable in some places on Tinos. Stretching lineation and brittle strain axes indicate a continuum of strain from ductile to brittle on the two islands (Mehl *et al.* 2005). Extension is oriented NE–SW.

Drawing two cross-sections of Tinos and Andros perpendicular to the detachment allows us to further compare the spatial evolution of deformation (Fig. 14). The two islands show the same gradient of retrogression from SW to NE, with better-preserved HP parageneses on the southern coast. Peak P–T conditions, although not well constrained on Andros, seem to be comparable, at 18 or 15 kbar and 500 °C for Tinos (Parra *et al.* 2002) and $>$10 kbar and 450–500 °C for Andros. The greenschist overprint is estimated at 9 kbar and 400 °C for Tinos (Parra *et al.* 2002) and 5–6 kbar and 400 °C for Andros (Reinecke 1982). Andros seems *a priori* to have undergone lower pressures than Tinos for equivalent temperatures, but, again, we must remain cautious with this conclusion: contrary to Tinos where precise P–T estimates were

made, $P-T$ estimates on Andros are based on only one metamorphic reaction.

The same gradient of shear strain exists on the two islands, with a coaxial flow on the southwestern part of the islands, which evolves towards a non-coaxial flow when approaching the detachment, as indicated by the evolution from a symmetrical deformation on the SW coast towards an asymmetric deformation on the NE coast. Symmetrical deformation is expressed in a wide southern zone on Andros whereas it is limited to a narrow band on the southern coast of Tinos. However, the different widths of the two islands, and therefore the difference in area of outcrops away from the detachment, may cause a bias in these observations.

Some structural differences exist between the two islands. Ductile structures, and especially decametre-scale shear bands, are better expressed on Andros than on Tinos, and they are more 'brittle' there. The decametre-scale shear bands of Andros seem to have been frozen during the localization process and to have encompassed brittle deformation, whereas on Tinos the whole NE part of the island below the main detachment is a large-scale shear zone with a large concentration of strain. The progressive evolution with increasingly numerous shear bands seen on Andros is not as clearly visible on Tinos, where the spatial transition from coaxial to non-coaxial is more abrupt. We interpret this observation as the result of a greater strain localization and a larger finite strain for Tinos. This interpretation is in agreement with the fact that Tinos is closer to the centre of the Cyclades, where extension has its maximum rate, and closer to Mykonos and Naxos, where the units that have experienced the highest temperatures have been exhumed (migmatites) (Avigad & Garfunkel 1989; Jolivet & Patriat 1999).

A study was made on the boudins of the two islands, because they testify for the amount to finite strain the rocks encompassed from the beginning of the greenschist overprint to the end of the localization process. We analysed 39 photographs of trains of boudins of different scales and in different material, taken in the maximum stretching plane. Twenty-one photographs were taken on Andros, and 18 on Tinos. Assuming a conservation of surface, we transform them into trains of rectangles whose heights correspond to the maximum height of the initial trains of boudins (Fig. 15, 1–3). We used the strain reversal program (Lloyd & Condliffe 2003) to constrain the elongation coefficient responsible for the boudinage (Fig. 15, 4). Results are presented in Figure 15, 5. The peaks of frequency of elongation coefficient are between 300 and 400% and 200 and 300% and the means of the elongation coefficients are 412% and 245% for Tinos and Andros, respectively. Despite the roughness of these estimates, it can be proposed that Tinos recorded, at least until boudinage started, a greater finite strain than Andros, thus supporting conclusions derived solely from field observations. The peak of greenschist overprint is dated to 21–23 Ma on Tinos (Avigad & Garfunkel 1989; Stolz *et al.* 1997). Assuming boudinage to be coeval with greenschist deformation and the peaks being nearly coeval on Andros and Tinos, it is possible to calculate the mean strain rate rocks sustained: it is roughly evaluated $4.5e-15\ s^{-1}$ for Tinos and $2.1e-15\ s^{-1}$ for Andros.

The fact that the shear bands of Andros were 'frozen' could perhaps have been favoured by an earlier arrival of Andros in the brittle domain. A gradient of the P/T ratios from Mt. Olympus to Naxos has been proposed by Jolivet & Patriat (1999) by comparison of the $P-T$ paths of the islands. A first-order estimation of the gradients of temperature in the final part of the $P-T$ paths gives $20\ ^{\circ}C\ km^{-1}$, $30\ ^{\circ}C/km$ and $40\ ^{\circ}C\ km^{-1}$ for Olympus, Tinos and Naxos, respectively. These gradients seem very large, but a systematic increase of the P/T ratios in the shallower part of the crust (i.e. the depths around the brittle–ductile transition zone) can be deduced from the $P-T$ paths. As Andros is situated between Olympus and Tinos, it seems logical to consider its P/T ratio to be between 20 and $30\ ^{\circ}C\ km^{-1}$. Because no $P-T$ paths have been precisely calculated on Andros, it is difficult to confirm this hypothesis without doubt. We further assume that P/T ratios seen on the $P-T$ grid give an idea of geothermal gradients.

As strain rate estimates on the two islands are not significantly different and the P/T ratios of Andros are probably less important than those of Tinos, we can hypothesize that the brittle–ductile transition zone of Andros develops at deeper levels of the crust than that of Tinos: this could explain why the shear bands of Andros seem more brittle than those of Tinos.

Furthermore, the brittle evolution is furthermore different on Tinos and Andros. Tinos seems to have recorded an episode of semi-brittle to brittle deformation that Andros has not: small-scale shallow-dipping normal faults were found in the footwall of Tinos (Mehl *et al.* 2005) that never appear on Andros below the detachment. In contrary, Andros has preserved one early stage of brittle deformation that Tinos does not: en echelon arrays of veins are well preserved in metabasitic and quartzitic lithologies of Andros, whereas actual faults are the rule on Tinos. These differences tend to prove that the localization process is more mature on Tinos than on Andros.

No major tilting of structures has been recorded on Tinos, as pointed out by the inversion of stress

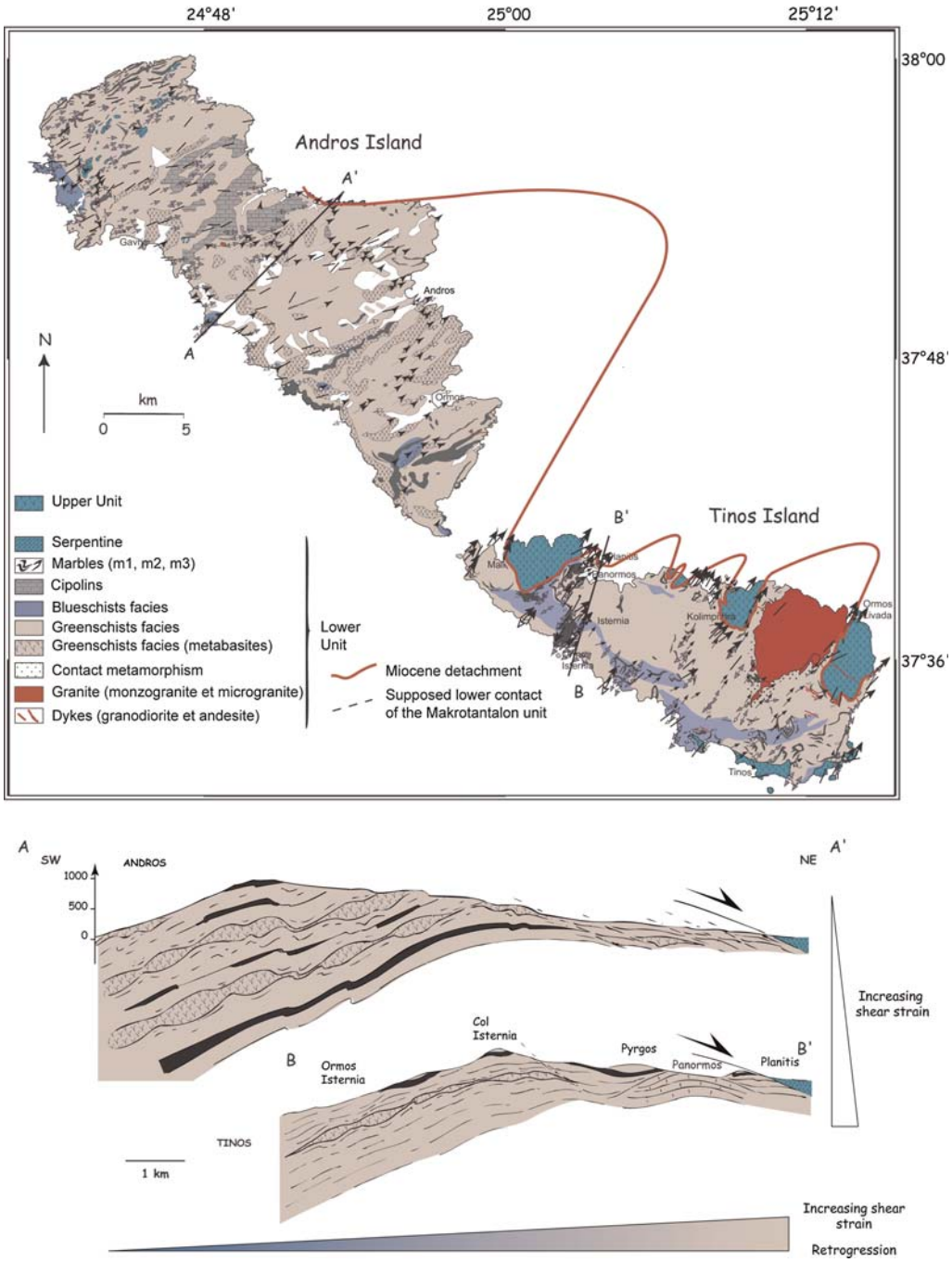

Fig. 14. Comparison in map and cross-section of Tinos and Andros. The two islands display the same gradients of retrogression and increasing shear strain from SW to NE. Decametre-scale shear bands are better preserved on Andros. We interpret this as the result of greater strain localization and larger finite strain for Tinos.

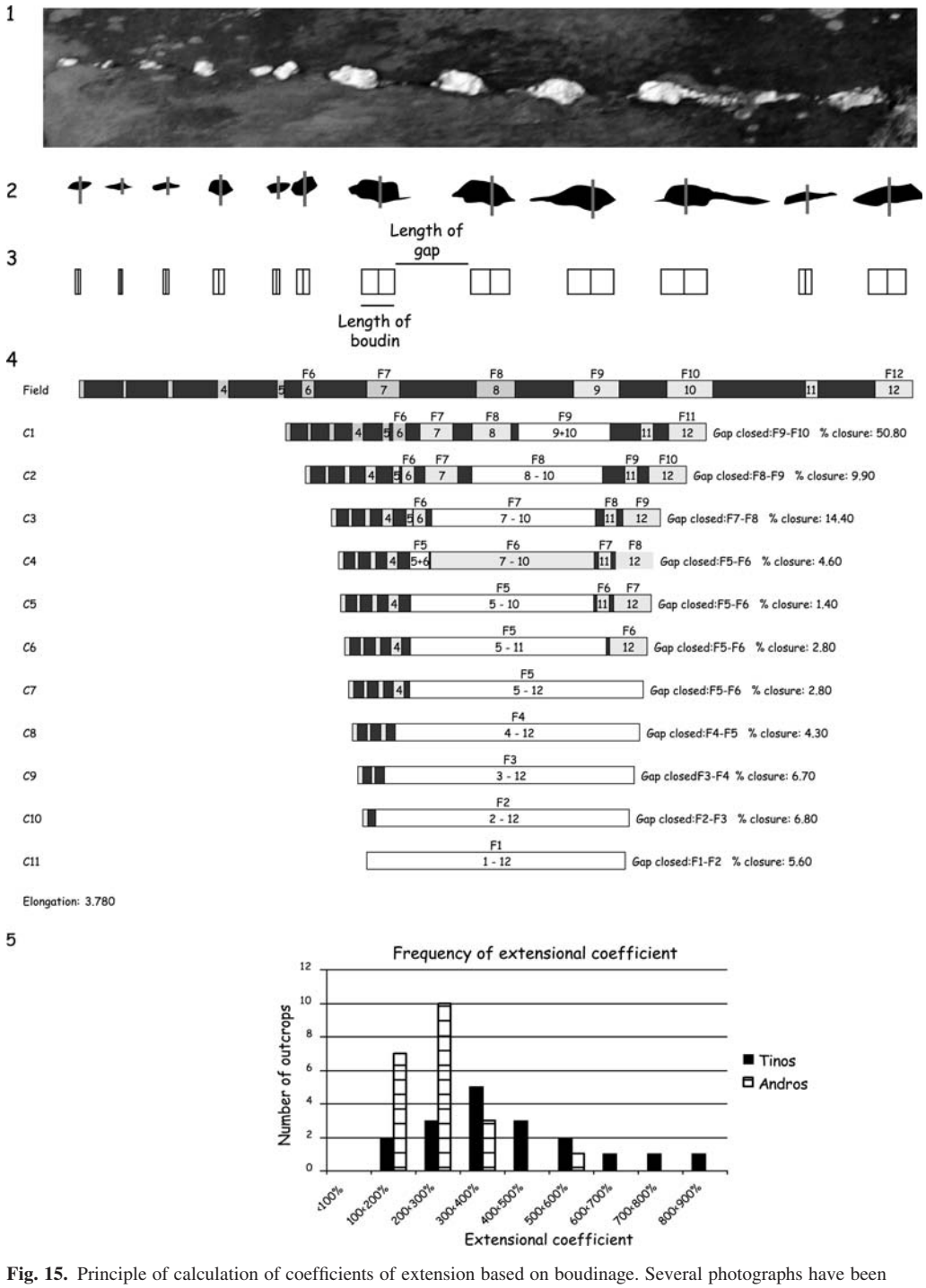

Fig. 15. Principle of calculation of coefficients of extension based on boudinage. Several photographs have been analysed for Tinos and Andros. The first step consists of calculating the surface of the trains of boudins. Assuming a conservation of surface, the boudins were replaced by rectangles whose position on a horizontal was deduced from the position of the maximum high of each boudin. The coefficient of elongation was computed from the Strain Reversal Program® (Lloyd & Condliffe 2003). The extensional coefficients of the two islands are shown in the lower part of the figure.

tensor. σ_1 is vertical or close to vertical for the major part of the studied outcrops, in good agreement with the ubiquitous vertical attitude of veins all over the island (Mehl *et al.* 2005). This absence of tilting is confirmed by the palaeomagnetic data on the granodiorite and on post-folial dykes of Tinos (Morris & Anderson 1996; Avigad *et al.* 1998). The major part of extension was accommodated before 19 Ma on Tinos, which corresponds to the age of the granite intrusion, and the post-ductile extension was also achieved without tilting. All brittle structures of Andros have similarly formed under a vertical maximum stress axis σ_1, but contrary to the major part of the outcrops of Tinos, they have been locally tilted in a late stage of deformation, probably in response to large-scale open NE–SW folds (Papanikolaou 1978; Avigad *et al.* 2001).

Conclusion: toward a complete section of an extending continental crust

Our observations on Andros and Tinos show two different stages of a continuous process that exhumed metamorphic rocks below a crustal-scale detachment. Earlier stages can be seen near Mt. Olympus and on the island of Evia, and a later and extreme stage on Mykonos and Naxos (Jolivet & Patriat 1999). As proposed by Avigad & Garfunkel (1989), deeper units are exhumed from Evia to Mykonos. This observation led those workers to postulate a NW–SE direction of extension, before the deformation was first described by Gautier (1994) and the top-to-the-NE shear sense ascertained. We assume that the same extension process has caused Oligo-Miocene post-HP exhumation from Mt. Olympus to Mykonos–Naxos during the formation of the Aegean Sea and that the only difference lies in the finite extension, which is greater in the centre of the Cyclades. An active equivalent of this deformation process can be found along the NE coast of continental Greece (Laigle *et al.* 2000) and in the Gulf of Corinth (Jolivet *et al.* 1994; Jolivet 2001), where brittle faults roots on shallow north- or NE-dipping shear zones within the brittle–ductile transition (Rigo *et al.* 1996; Sorel 2000). Following this assumption we can propose a scheme of vertical stratification of deformation regimes from the extending upper brittle crust to the lower crust (Fig. 16).

The following rheological stratification is proposed. (1) The upper crust is brittle and shallow- and steeply dipping normal faults control the deposition of synrift basins. (2) Cataclastic deformation along the main detachment allows it to continue with a shallow dip for most of its life (Mehl *et al.* 2005). The cataclastic shear zone becomes wider downward and a progressive change to ductile conditions is observed depending on the nature of the material involved and the thermal and fluid conditions. (3) At depth this shear zone becomes shallow dipping and merges with a shallow NE-dipping shear zone below the brittle–ductile transition. (4) The lower crust is weak because of partial melting as recorded on Mykonos or Naxos and the deformation is thus less localized. The deformation there is thus partitioned between bulk coaxial thinning and simple shear induced by the motion of the hanging wall of the detachment.

At the brittle–ductile transition, the deformation is progressively localized in the footwall, first in the necks between boudins and along shear zones. An evolution toward more non-coaxial conditions is observed toward the detachment. The overall structure corresponds to a megaboudinage of the crust with the localization of a shear zone and then a fault at the extremity of this crustal-scale boudin.

This evolution thus emphasizes that the rheological stratification and the intrinsic compositional heterogeneity of the continental crust (leading to boudinage) both control strain localization processes. This process is, furthermore, under the control of the behaviour of fluids. Famin *et al.* (2004) have shown that surface-derived fluids invade the brittle–ductile transition and favour strain localization at this level of the crust. A connected vein network ensures the channelization of these fluids from the surface, along the uppermost faults and within the brittle–ductile transition. Further down, veins do not make a connected network and fluid accumulate at the brittle–ductile transition. The presence of these fluids in active extensional context is well illustrated by the Corinth Rift case (Pham *et al.* 2000). As mentioned above, fluids can lower the resistance of the rocks and favour strain localization but they need the formation of conduits to reach the brittle–ductile transition, they thus need some strain localization to have already happened. This early strain localization, as shown on Andros, can be explained by boudinage and the formation of shear bands and faults in the necks between boudins. Andros illustrates this stage, whereas Tinos shows the later evolution toward the formation of a narrow shear zone when an intense shearing is recorded. The latest stage of extension shows a more coaxial deformation pattern and is marked by widespread conjugate sets of steeply dipping mesoscale normal faults all over the islands. These faults cut across the cataclastic zone itself, indicating that this zone was no longer active at that time and that the cataclasites have become progressively stiffer and

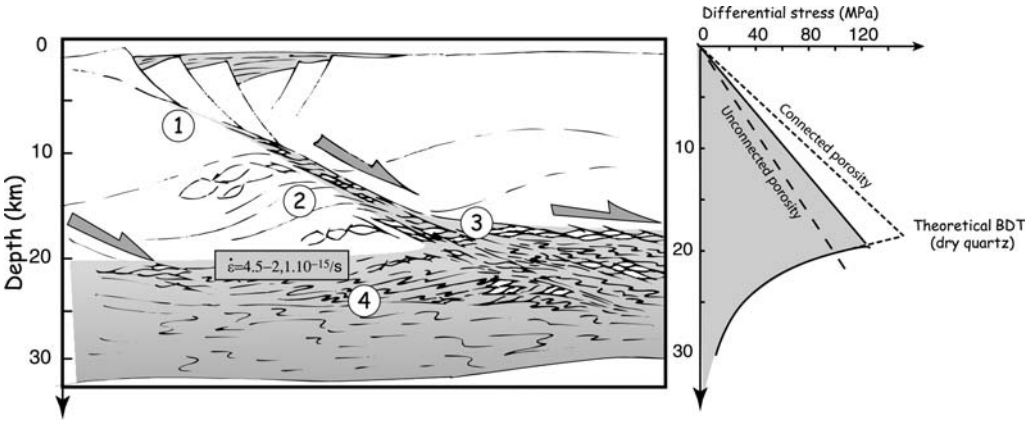

Fig. 16. Synthetic cross-section of an extending continental crust. (1) Brittle upper crust: shallow- and steeply dipping normal faults control the deposition of synrift basins. (2) The cataclastic shear zone broadens with depth, evolving progressively towards ductile deformation. (3) Decrease in the dip of the shear zone, which merges below the brittle–ductile transition (BDT). (4) Weak lower crust, as a result of partial melting. We show on the cross-section the strain rates calculated from boudinage on the islands of Tinos and Andros. A rheological envelope, calculated from the rheological parametres of dry quartz, is shown in the right part of the picture to better calibrate the depth scale of the cross-section.

more brittle during exhumation, while the shear movement localizes along the flat brittle detachment, which accommodates the last increments of extension.

References

ANGELIER, J. 1990. Inversion of field data in fault tectonics to obtain the regional stress—III. A new rapid direct inversion method by analytical means. *Geophysical Journal International*, **103**, 363–376.

ARMIJO, R., LYON-CAEN, H. & PAPANIKOLAOU, D. 1992. East–West extension and Holocene normal fault scarps in the Hellenic arc. *Geology*, **20**, 491–494.

ARMIJO, R., MEYER, B., KING, G. C. P., RIGO, A. & PAPANASTASSIOU, D. 1996. Quaternary evolution of the Corinth Rift and its implications for the Late Cenozoic evolution of the Aegean. *Geophysical Journal International*, **126**, 11–53.

AUBOUIN, J. & DERCOURT, J. 1965. Sur la géologie de l'Egée: regard sur la Crète (Grèce). *Bulletin de la Société Géologique de France*, **7**, 787–821.

AUGIER, R., JOLIVET, L. & ROBIN, C. 2005. Late Orogenic doming in the eastern Betic Cordilleras: Final exhumation of the Nevado-Filabride complex and its relation to basin genesis. *Tectonics*, **24**, doi: 10.1029/2004TC001687.

AVIGAD, D. & GARFUNKEL, Z. 1989. Low-angle faults above and below a blueschist belt: Tinos Island, Cyclades, Greece. *Terra Nova*, **1**, 182–187.

AVIGAD, D. & GARFUNKEL, Z. 1991. Uplift and exhumation of high-pressure metamorphic terranes: the example of the Cycladic blueschists belt (Aegean Sea). *Tectonophysics*, **188**, 357–372.

AVIGAD, A., GARFUNKEL, Z., JOLIVET, L. & AZAÑÓN, J. M. 1997. Back-arc extension and denudation of Mediterranean eclogites. *Tectonics*, **16**, 924–941.

AVIGAD, D., BAER, G. & HEIMANN, A. 1998. Block rotations and continental extension in the Central Aegean Sea: paleomagnetic and structural evidence from Tinos and Mykonos. *Earth and Planetary Science Letters*, **157**, 23–40.

AVIGAD, D., ZIV, A. & GARFUNKEL, Z. 2001. Ductile and brittle shortening, extension-parallel folds and maintenance of crustal thickness in the Central Aegean. *Tectonics*, **20**, 277–287.

BLAKE, M. C. J., BONNEAU, M., GEYSSANT, J., KIENAST, J. R., LEPVRIER, C., MALUSKI, H. & PAPANIKOLAOU, D. 1981. A geologial reconnaissance of the Cycladic blueschist belt, Greece. *Geological Society of America Bulletin*, **92**, 247–254.

BONNEAU, M. 1982. Evolution géodynamique de l'arc égéen depuis le Jurassique Supérieur jusqu'au Miocène. *Bulletin de la Société Géologique de France*, **7**, 229–242.

BOTT, M. H. P. 1959. The mechanisms of oblique slip faulting. *Geological Magazine*, **96**, 109–117.

BOZKURT, E. 2003. Origin of the NNE-trending basins in Westren Turkey. *Geodinamica Acta*, **16**, 61–81.

BOZKURT, E. & PARK, R. G. 1997. Evolution of a mid-Tertiary extensional shear zone in the southern Menderes massif, western Turkey. *Bulletin de la Société Géologique de France*, **168**, 3–14.

BRÖCKER, M. & FRANZ, L. 2006. Dating metamorphism and tectonic stacking on Andros Island (Cyclades, Greece): results of a Rb–Sr study. *Geological Magazine*, **143**, 609–620.

BRUNN, J. H., ARGYRIADIS, I., RICOU, L. E., POISSON, A., MARCOUX, J. & DE GRACIANSKY, P. C. 1976. Eléments majeurs de liaison entre Taurides et Hellénides. *Bulletin de la Société Géologique de France*, **18**, 481–497.

DAVIS, G. H. 1980. Structural characteristics of metamorphic core complexes, southern Arizona. *In*: CRITTENDEN, M. D. J., CONEY, P. J. & DAVIS, G. H.

(eds) *Cordilleran Metamorphic Core Complexes*. *Geological Society of America, Memoirs*, **153**, 35–77.

DAVIS, G. H. & CONEY, P. J. 1979. Geologic development of the Cordilleran metamorphic core complexes. *Geology*, **7**, 120–124.

DIXON, J. & WILLIAMS, G. 1983. Reaction softening in mylonites from Arnaboll thrust, Sutherland. *Scottish Journal of Geology*, **19**, 157–168.

DÜRR, S. 1986. Das Attisch-kykladische Kristallin. *In*: JACOBSHAGEN, V. (ed.) *Geologie von Grienchenland* Gebruder Borntraeger, Berlin, 116–148.

FAMIN, V., PHILIPPOT, P., JOLIVET, L. & AGARD, P. 2004. Evolution of hydrothermal regime along a crustal shear zone, Tinos Island, Greece. *Tectonics*, **23**, doi:10.1029/2003TC001509.

FAURE, M. & BONNEAU, M. 1988. Données nouvelles sur l'extension néogène de l'Egée: la déformation ductile du granite miocène de Mykonos (Cyclades, Grèce). *Comptes Rendus de l' Academie des Sciences*, **307**, 1553–1559.

FITZ GERALD, J. D. & STÜNITZ, H. 1993. Deformaton of granitoids at low metamorphic grade. Reactions and grain size reduction. *Tectonophysics*, **221**, 269–297.

GAUTIER, P. 1994. Géométrie crustale et cinématique de l'extension tardi-orogénique dans le domaine centre-égéen (iles des Cyclades et d'Eubée, Grèce). Unpublished Thesis, Université de Rennes.

GAUTIER, P. & BRUN, J. P. 1994*a*. Ductile crust exhumation and extensional detachments in the central Aegean (Cyclades and Evvia islands). *Geodinamica Acta*, **7**, 57–85.

GAUTIER, P. & BRUN, J. P. 1994*b*. Crustal-scale geometry and kinematics of late-orogenic extension in the central Aegean (Cyclades and Evvia island). *Tectonophysics*, **238**, 399–424.

GUEYDAN, F., LEROY, Y. & JOLIVET, L. 2001. Grain-size sensitive flow and shear stress enhancement at the brittle to ductile transition of the continental crust. *International Journal of Earth Sciences*, **90**, 181–196.

GUEYDAN, F., LEROY, Y., JOLIVET, L. & AGARD, P. 2003. Analysis of continental midcrustal strain localization induced by microfracturing and reaction-softening. *Journal of Geophysical Research*, **108**, 2064, doi:10.1029/2001JB000611.

JACOBSHAGEN, V., DÜRR, S., KOCKEL, F., KOPP, K. O., KOWALCZYK, G., BERCKHEMER, H. & BÜTTNER, D. 1978. Structure and geodynamic evolution of the Aegean region. *In*: CLOOS, H., ROEDER, D. & SCHMIDT, K. (eds) *Alps, Apennines, Hellenides*. IUGG, **report 38** Stuttgart, 537–564.

JACKSON, J. A. 1987. Active normal faulting and continental extension. *In*: COWARD, M. P., DEWEY, J. F. & HANCOCK, P. L. (eds) *Continental Extensional Tectonics*. Geological Society, London, Special Publications, **28**, 3–18.

JACKSON, J. 1994. Active tectonics of the Aegean region. *Annual Review of Earth and Planetary Sciences*, **22**, 239–271.

JACKSON, J. A. & WHITE, N. J. 1989. Normal faulting in the upper continental crust: observations from regions of active extension. *Journal of Structural Geology*, **11**, 15–36.

JOLIVET, L. 2001. A comparison of geodetic and finite strain pattern in the Aegean, geodynamic implications. *Earth and Planetary Science Letters*, **187**, 95–104.

JOLIVET, L. & FACCENNA, C. 2000. Mediterranean extension and the Africa–Eurasia collision. *Tectonics*, **19**, 1095–1106.

JOLIVET, L. & PATRIAT, M. 1999. Ductile extension and the formation of the Aegean Sea. *In*: DURAND, B., JOLIVET, L., HORVÀTH, F. & SÉRANNE, M. (eds) *The Mediterranean Basins: Tertiary Extension within the Alpine Orogen*. Geological Society, London, Special Publications, **156**, 427–456.

JOLIVET, L., BRUN, J. P., GAUTIER, P., LALLEMANT, S. & PATRIAT, M. 1994. 3-D kinematics of extension in the Aegean from the Early Miocene to the Present, insight from the ductile crust. *Bulletin de la Société Géologique de France*, **165**, 195–209.

JOLIVET, L., FAMIN, V., MEHL, C., PARRA, T., AVIGAD, D. & AUBOURG, C. 2004*a*. Progressive strain localisation, crustal-scale boudinage and extensional metamorphic domes in the Aegean Sea. *In*: WHITNEY, D. L., TEYSSIER, C. & SIDDOWAY, C. S. (eds) *Gneiss Domes in Orogens*. American Geological Society, Special Papers, **380**, 185–210.

JOLIVET, L., RIMMELÉ, G., OBERHÄNSLI, R., GOFFÉ, B. & CANDAN, O. 2004*b*. Correlation of syn-orogenic tectonic and metamorphic events in the Cyclades, the Lycian Nappes and the Menderes massif, geodynamic implications. *Bulletin de la Société Géologique de France*, **175**, 217–238.

KATZIR, Y., AVIGAD, D., MATTHEWS, A., GARFUNKEL, Z. & EVANS, B. 2000. Origin, HP/LT metamorphism and cooling of ophiolitic mélanges in southern Evia (NW Cyclades), Greece. *Journal of Metamorphic Geology*, **18**, 699–718.

KIRBY, S. H. 1985. Rock mechanics observations pertinent to the rheology of the continental lithosphere and the localization of strain along shear zones. *Tectonophysics*, **119**, 1–27.

LAIGLE, M., HIRN, A., SACHPAZI, M. & ROUSSOS, N. 2000. North Aegean crustal deformation: an active fault imaged to 10 km depth by reflection seismic data. *Geology*, **28**, 71–74.

LE PICHON, X. & ANGELIER, J. 1981. The Aegean Sea. *Philosophical Transaction of the Royal Society of London*, **300**, 357–372.

LISTER, G. S. & DAVIS, G. A. 1989. The origin of metamorphic core complexes and detachment faults formed during Tertiary continental extension in the northern Colorado River region, U.S.A. *Journal of Structural Geology*, **11**, 65–94.

LISTER, G. S., BANGA, G. & FEENSTRA, A. 1984. Metamorphic core complexes of cordilleran type in the Cyclades, Aegean Sea, Greece. *Geology*, **12**, 221–225.

LLOYD, G. E. & CONDLIFFE, E. 2003. 'Strain Reversal': a Windows™ program to determine extensional strain from rigid–brittle layers or inclusions. *Journal of Structural Geology*, **25**, 1141–1145.

MARQUER, D., GAPAIS, D. & CAPDEVILA, R. 1985. Chemical changes and mylonitisation of a granodiorite within low-grade metamorphism (Aar Massif, Central Alps). *Bulletin de Minéralogie*, **108**, 209–221.

MEHL, C., JOLIVET, L. & LACOMBE, O. 2005. From ductile to brittle: evolution and localization of deformation below a crustal detachment (Tinos, Cyclades, Greece). *Tectonics*, **24**, TC4017, doi: 10.1029/2004TC001767.

MITRA, G. 1978. Ductile deformation zones and mylonites: the mechanical processes involved in the deformation of crystalline basement rocks. *American Journal of Science*, **278**, 1057–1084.

MORRIS, A. & ANDERSON, A. 1996. First paleaomagnetic results from the Cycladic Massif, Greece, and their implications for Miocene extension directions and tectonic models in the Aegean. *Earth and Planetary Science Letters*, **142**, 397–408.

PAPANIKOLAOU, D. J. 1978. Contribution to the geology of the Aegean Sea: the island of Andros. *Annales Géologiques des Pays Helléniques*, **29**, 477–553.

PAPANIKOLAOU, D. 1987. Tectonic evolution of the Cycladic blueschist belt (Aegean Sea, Greece). *In*: HELGESON, H. C. (ed.) *Chemical Transport in Metasomatic Processes*. D. Reidel Publishing Company, Dordrecht, 429–450.

PAPANIKOLAOU, D., LYKOUSIS, V., CHRONIS, G. & PAVLAKIS, P. 1988. A comparative study of neotectonic basins across the Hellenic arc: the Messiniakos, Argolikos, Saronikos and Southern Evoikos gulfs. *Basin Research*, **1**, 167–176.

PARRA, T., VIDAL, O. & JOLIVET, L. 2002. Relation between deformation and retrogression in blueschist metapelites of Tinos island (Greece) evidenced by chlorite–mica local equilibria. *Lithos*, **63**, 41–66.

PATRIAT, M. 1996. Etude de la transition cassant-ductile en extension, application au transect Olympe-Naxos, Grèce. Unpublished Thèse de Doctorat, Université Pierre et Marie Curie, Paris.

PATRIAT, M. & JOLIVET, L. 1998. Post-orogenic extension and shallow-dipping shear zones, study of a brecciated décollement horizon in Tinos (Cyclades, Greece). *Comptes Rendus de l'Académie des Sciences*, **326**, 355–362.

PHAM, V. N., BERNARD, P., BOYER, D., CHOULIARAS, G., LE MOUEL, J. L. & STAVRAKAKIS, G. N. 2000. Electrical conductivity and crustal structure beneath the central Hellenides around the Gulf of Corinth (Greece) and their relationship with the seismotectonics. *Geophysical Journal International*, **142**, 948–969.

PRICE, N. J. & COSGROVE, J. W. 1990. Boundinage and pinch-and-swell structures. *In*: PRICE, N. J. & COSGROVE, J. W. *Analysis of Geological Structures*. Cambridge University Press, Cambridge, 405–443.

REINECKE, T. 1982. Cymrite and celsian in manganese-rich metamorphic rocks from Andros island, Greece. *Contributions to Mineralogy and Petrology*, **79**, 333–336.

REINECKE, T. 1986. Phase relationships of sursassite and other Mn-silicates in highly oxidized low-grade, high-pressure metamorphic rocks from Evvia and Andros Islands, Greece. *Contributions to Mineralogy and Petrology*, **84**, 110–126.

REINECKE, T., OKRUSCH, M. & RICHTER, P. 1985. Geochemistry of ferromanganoan metasediments from the island of Andros, Cycladic Blueschist Belt, Greece. *Chemical Geology*, **53**, 249–278.

RIETBROCK, A., TIBÉRI, C., SCHERBAUM, F. & LYON-CAEN, H. 1996. Seismic slip on a low angle normal fault in the Gulf of Corinth: evidence from high resolution cluster analysis of microearthquakes. *Geophysical Research Letters*, **23**, 1817–1820.

RIGO, A., LYON-CAEN, H., ARMIJO, R. *ET AL*. 1996. A microseismicity study in the western part of the Gulf of Corinth (Greece): implications for large-scale normal faulting mechanisms. *Geophysical Journal International*, **126**, 663–688.

SEYITOGLU, G. & SCOTT, B. 1991. Late Cenozoic crustal extension and basin formation in West Turkey. *Geological Magazine*, **128**, 155–166.

SEYITOGLU, G. & SCOTT, B. C. 1996. The cause of N–S extensional tectonics in western Turkey: tectonic escape vs back-arc spreading vs orogenic collapse. *Journal of Geodynamics*, **22**, 145–153.

SHAKED, Y., AVIGAD, D. & GARFUNKEL, Z. 2000. Alpine high-pressure metamorphism at the Almyropotamos window (southern Evia, Greece). *Geological Magazine*, **137**, 367–380.

SOREL, D. 2000. A Pleistocene and still-active detachment fault and the origin of the Corinth–Patras rift, Greece. *Geology*, **28**, 83–86.

STOLZ, J., ENGI, M. & RICKLI, M. 1997. Tectonometamorphic evolution of SE Tinos, Cyclades, Greece. *Swiss Bulletin of Mineralogy and Petrology*, **77**, 209–231.

TAYMAZ, T., JACKSON, J. & MCKENZIE, D. 1991. Active tectonics of the north and central Aegean Sea. *Geophysical Journal International*, **106**, 433–490.

TAYMAZ, T., WESTAWAY, R. & REILINGER, R. (eds) 2004. Active faulting and crustal deformation in the Eastern Mediterranean Region. *Tectonophysics* (special issue), **391**.

WALLACE, R. E. 1951. Geometry of shearing stress andrelation to faulting. *Journal of Geology*, **59**, 118–130.

WEATHERS, M. S., BIRD, J. M., COOPER, R. F. & KOHLSTEDT, D. L. 1979. Differential stress determined from deformation-induced microstructures of the Moine Thrust Zone. *Journal of Geophysical Research*, **84**, 7495–7509.

WHITE, S. H. & KNIPE, R. J. 1978. Transformation- and reaction-enhanced ductility in rocks. *Journal of the Geological Society, London*, **135**, 513–516.

WIBBERLY, C. 1999. Are feldspar-to-micas reactions necessarily reaction-softening process in fault zones? *Journal of Structural Geology*, **21**, 1219–1227.

WINTSCH, R. P., CHRISTOFFERSEN, R. & KRONENBERG, A. K. 1995. Fluid–rock reaction weakening of fault zones. *Journal of Geophysical Research*, **100**, 13021–13032.